Biexciton states in semiconductor quantum dots and their nonlinear optical properties

T. Takagahara
NTT Basic Research Laboratories, Musashino-shi, 180 Tokyo, Japan
(Received 19 September 1988; revised manuscript received 28 November 1988)

Biexciton states in semiconductor quantum dots (spherical microcrystallites) are investigated variationally, and the biexciton binding energy and the oscillator strength are calculated as a function of the quantum-dot radius, the electron-to-hole mass ratio, and the dielectric constant ratio of the semiconductor to the surrounding medium. The most important mechanisms for enhancing the biexciton binding energy and the oscillator strength are clarified. One is the quantum confinement effect, which increases the spatial overlap between carriers, leading to enhanced Coulomb interaction. Another is the dielectric confinement effect due to the dielectric constant discontinuity at the interface between a semiconductor microcrystallite and the surrounding medium. This effect arises from the penetration of electric force lines through the surrounding medium with a relatively small dielectric constant and leads to an enhancement of the Coulomb interaction. It is found that the frequency dispersion of the third-order nonlinear susceptibility $\chi^{(3)}$ shows an out-of-phase behavior at the one- and two-photon resonances, which is characteristic of the exciton and biexciton transitions. For typical materials which are promising for observation of the biexciton state in microcrystallites, the values of the biexciton binding energy, the third-order nonlinear susceptibility $\chi^{(3)}$, and the two-photon absorption coefficient K_2 of the biexciton state are predicted theoretically.

I. INTRODUCTION

Recently the excitonic states in semiconductor microstructures have attracted much attention from the fundamental physics viewpoint and also from the interest of applied physics, owing to enhanced excitonic optical nonlinearity and fast response time.[1–16] In semiconductor microstructures of lower dimensionality, the energy levels of carriers become discrete due to the quantum confinement effect. At the same time, the oscillator strength, which is distributed over continuum states in bulk materials, becomes concentrated on the sharp transitions of excitons and consequently the excitonic optical nonlinearity becomes enhanced and the saturation power becomes reduced relative to those of the bulk semiconductor. On the other hand, the biexciton state in semiconductor microstructures has not yet received much attention. The biexciton state in two-dimensional quantum-well structures was investigated theoretically several years ago.[17] However, it was not until recently that the biexciton state was observed convincingly in II-VI compound semiconductor quantum wells.[18] The biexciton state in one-dimensional quantum wire structures was recently studied theoretically and the enhancement of biexciton binding energy was predicted.[19]

In semiconductor microstructures of lower dimensionality, the spatial overlap between an electron and a hole is increased, leading to the increase in the Coulomb binding energy and the oscillator strength. As an ultimate limit of the reduced dimensionality, the zero-dimensional materials such as semiconductor microcrystallites are expected to show a much more enhanced binding energy of the biexciton state and to have an enhanced oscillator strength of the two-photon generation of the biexciton state. However, in the case of the biexciton state, the Coulomb repulsion between like particles, namely two electrons and two holes, is also enhanced in microstructures. Thus the biexciton binding energy is not enhanced straightforwardly as the particle size is reduced but is dependent on a delicate balance between the Coulomb attraction and the Coulomb repulsion. Furthermore, in actual samples of semiconductor microcrystallites such as $CdS_{1-x}Se_x$ in glass and CuCl in NaCl, the difference of dielectric constants between the microcrystallites and the surrounding medium is rather large. The significance of the dielectric constant discontinuity at an interface in enhancing the Coulomb interaction was first pointed out by Keldysh.[20] It is found recently that in two-dimensional quantum-well structures the exciton binding energy and its oscillator strength depend sensitively on the dielectric constant ratio between the well and barrier materials.[21] While the electrons and holes are confined within a quantum well, the electric force lines among electrons and holes pass through the surrounding medium with a relatively small dielectric constant. As a result, the screening effect is reduced and the Coulomb interaction among electrons and holes is enhanced to yield a large binding energy. The same situation holds also in the zero-dimensional materials.[22] Thus the effect of the dielectric constant discontinuity, which will be referred to as the dielectric confinement effect hereafter, should be taken into account in the calculation of the biexciton binding energy.

Recently Banyai *et al.*[23] reported a calculation of the biexciton resonance in a GaAs quantum dot employing the adiabatic approximation in which the electron motion is frozen in. Their calculation seems to suggest a negative biexciton binding energy, namely repulsive exciton-exciton interaction for the moderate confinement regime. However, the adiabatic approximation is too simple to

take into account the correlation among two electrons and two holes. Here we employ a more elaborate variational approach to incorporate fully the four-particle correlation and investigate systematically the dependence of the biexciton binding energy and the oscillator strength on the quantum-dot radius, the electron-to-hole mass ratio, and the dielectric constant ratio between the quantum-dot material and the surrounding medium. It is found that the dielectric confinement effect plays an important role in enhancing the biexciton binding energy even for the moderate confinement regime.

The biexciton state consists of two excitons and is known to have a giant oscillator strength for two-photon generation.[24] Thus the optical nonlinearity via the biexciton state is expected to be enhanced by the giant oscillator strength. At the same time, the frequency dispersion of the third-order nonlinear susceptibility is expected to show a characteristic behavior at the two-photon resonance different from that at the one-photon resonance. These features will be discussed in detail in the text. Furthermore, since the nonlinearity arises from the two-photon coherence instead of the saturation of exciton population, the response time of this nonlinearity is expected to be very fast.

In Sec. II, the relevant Hamiltonian is given for the biexciton state, namely for two electrons and two holes in the effective-mass approximation, and in Sec. III, details of variational calculation are presented. The results on the biexciton binding energy and the oscillator strength are given in Secs. IV and V. The nonlinear optical properties and the two-photon absorption of the biexciton state are discussed in Sec. VI. Typical materials which are promising for observing the biexciton state in microcrystallites are given in Sec. VII and their third-order nonlinear susceptibilities and two-photon absorption coefficients are estimated.

II. FORMULATION

The lowest state of a biexciton in a semiconductor quantum dot will now be investigated. It is now well known that the effective-mass approximation is applicable even for semiconductor microcrystallites containing only as few as 100 atoms.[25] Then the relevant Hamiltonian for two electrons and two holes is given as

$$
\begin{aligned}
H=&-\frac{\hbar^2}{2m_e}(\nabla_1^2+\nabla_2^2)-\frac{\hbar^2}{2m_h}(\nabla_a^2+\nabla_b^2)-\frac{e^2}{\epsilon_1|r_1-r_a|}-\frac{e^2}{\epsilon_1|r_1-r_b|}-\frac{e^2}{\epsilon_1|r_2-r_a|}-\frac{e^2}{\epsilon_1|r_2-r_b|}\\
&+\frac{e^2}{\epsilon_1|r_1-r_2|}+\frac{e^2}{\epsilon_1|r_a-r_b|}+\frac{e^2}{2R}\sum_{n=1}^{\infty}\alpha_n\left[\left[\frac{r_1}{R}\right]^{2n}+\left[\frac{r_2}{R}\right]^{2n}+\left[\frac{r_a}{R}\right]^{2n}+\left[\frac{r_b}{R}\right]^{2n}\right]\\
&-\frac{e^2}{R}\sum_{n=1}^{\infty}\alpha_n\left[\left[\frac{r_1r_a}{R^2}\right]^n P_n(\cos\theta_{1a})+\left[\frac{r_1r_b}{R^2}\right]^n P_n(\cos\theta_{1b})+\left[\frac{r_2r_a}{R^2}\right]^n P_n(\cos\theta_{2a})\right.\\
&\left.+\left[\frac{r_2r_b}{R^2}\right]^n P_n(\cos\theta_{2b})-\left[\frac{r_1r_2}{R^2}\right]^n P_n(\cos\theta_{12})-\left[\frac{r_ar_b}{R^2}\right]^n P_n(\cos\theta_{ab})\right] . \qquad (2.1)
\end{aligned}
$$

Here R is the radius of the quantum dot, r_a and r_b (r_1 and r_2) denote the coordinates of holes (electrons), and m_h (m_e) is the mass of hole (electron). The dielectric constant of the quantum dot and the surrounding medium is denoted by ϵ_1 and ϵ_2, respectively, and α_n is defined by

$$\alpha_n=\frac{(n+1)(\epsilon-1)}{\epsilon_1(n\epsilon+n+1)} , \qquad (2.2)$$

with $\epsilon=\epsilon_1/\epsilon_2$. P_n is the Legendre polynomial of the nth order and θ_{ij} is the angle between r_i and r_j. The first four terms represent the kinetic energy and the next six terms are the direct Coulomb energies among two electrons and two holes. The remaining ten terms represent the interaction energy among four particles and their image charges. The first four terms of these ten terms are the self-image potentials of four particles due to their image charges and the next six terms are the mutual image potentials among four particles and their image charges. This Hamiltonian is a natural extension of the exciton Hamiltonian[4] to the biexciton case.

To find out the lowest state of the four particles, a variational wave function is employed as

$$
\begin{aligned}
\Phi_m(r_1,r_2,r_a,r_b)=&\,C_m j_0(\pi r_1/R)j_0(\pi r_2/R)j_0(\pi r_a/R)j_0(\pi r_b/R)r_{ab}^{\gamma}\exp(-\delta r_{ab})\\
&\times\{\exp[-\alpha(r_{1a}+r_{2b})-\beta(r_{1b}+r_{2a})]+\exp[-\beta(r_{1a}+r_{2b})-\alpha(r_{1b}+r_{2a})]\} , \qquad (2.3)
\end{aligned}
$$

where $r_{ij}=|r_i-r_j|$, j_0 is the zeroth-order spherical Bessel function, C_m is the normalization constant, and α, β, γ, and δ are variational parameters to minimize the energy, namely

$$E_{XX}=\langle\Phi_m|H|\Phi_m\rangle/\langle\Phi_m|\Phi_m\rangle . \qquad (2.4)$$

In the energy-level scheme, two electrons and two holes occupy the lowest subband states forming a spin-singlet pair, respectively. Thus the spatial part of the wave function is symmetric with respect to the exchange of two holes or two electrons. The first four factors in (2.3)

stand for the lowest subband states in a spherical quantum dot whose wave function vanishes at the surface. This boundary condition is reasonable since the energy-gap difference between the quantum-dot material and the surrounding medium is rather large in actual samples. The wave function describing the relative motion among four particles is taken to be identical with that employed by Akimoto and Hanamura.[26] It is implicitly assumed that the quantum-dot size is so small that the quantum confinement energy is larger than the Coulomb energy among electrons and holes. Thus the above variational wave function is most suitable for the case of strong confinement. For larger quantum dots, we should include higher-lying subband states in the variational wave function. However, in the case of excitonic state, an elaborate calculation including higher-energy subband levels shows that the simplest wave function composed of the lowest subband states still gives a good estimate of various quantities even for the moderate confinement regime.[22] Thus it can be expected that the wave function (2.3) can give a reasonable description even for the moderate confinement regime. In the above variational wave function the electrons and holes are not handled symmetrically and thus the zero slope of physical quantities, e.g., biexciton binding energy, with respect to the change of the electron-to-hole mass ratio at the positronium limit ($m_e=m_h$) is not assured. However, since the electron-to-hole mass ratio is rather small in actual materials, the above variational wave function is sufficiently accurate to yield reliable estimates of physical quantities.

III. CALCULATION OF VARIOUS INTEGRALS

In this section, calculational details of various integrals which appear in (2.4) are presented. In the calculation of the matrix elements, it is convenient to introduce the Fourier transform of an exponential function as

$$\exp(-\alpha r_{ij})=\int d^3k\, e^{i\mathbf{k}\cdot(\mathbf{r}_i-\mathbf{r}_j)}g(k,\alpha)\ , \tag{3.1}$$

$$\frac{\exp(-\alpha r_{ij})}{r_{ij}}=\int d^3k\, e^{i\mathbf{k}\cdot(\mathbf{r}_i-\mathbf{r}_j)}f(k,\alpha)\ . \tag{3.2}$$

For a positive value of α, g and f are given as

$$g(k,\alpha)=\frac{\alpha}{\pi^2(k^2+\alpha^2)^2}\ , \tag{3.3}$$

$$f(k,\alpha)=\frac{1}{2\pi^2(k^2+\alpha^2)}\ . \tag{3.4}$$

In the bulk semiconductor, the four parameters α, β, γ, and δ in (2.3) are usually supposed to be positive to inhibit the wave function from becoming infinitely large. In a semiconductor quantum dot, however, there is no reason to believe that these parameters are all positive, because carriers are confined three dimensionally. In fact, as will be mentioned later, the parameter β turns out to be negative for many combinations of the physical parameters. For a negative value of α, these functions and related integrals are given in Appendix D. As for the interhole wave function $r_{ab}^{\gamma}e^{-\delta r_{ab}}$, γ should be positive physically to take into account the hole-hole repulsion, and δ turns out to be positive in the variational calculation. Then its Fourier transform is simply given by

$$r^{\gamma}e^{-\delta r}=\int d^3k\, e^{i\mathbf{k}\cdot\mathbf{r}}h(k,\gamma,\delta)\ , \tag{3.5}$$

with

$$h(k,\gamma,\delta)=\frac{\Gamma(2+\gamma)}{(2\pi)^2 ik}\left[\frac{1}{(\delta-ik)^{2+\gamma}}-\frac{1}{(\delta+ik)^{2+\gamma}}\right]\ . \tag{3.6}$$

A. Calculation of normalization integral

To illustrate the details of calculation, we shall take up a typical term in $\langle\Phi_m|\Phi_m\rangle$, namely

$$\int d^3r_1\int d^3r_2\int d^3r_a\int d^3r_b j_0^2(k_1^0r_1)j_0^2(k_1^0r_2)j_0^2(k_1^0r_a)j_0^2(k_1^0r_b)r_{ab}^{2\gamma}e^{-2\delta r_{ab}}\exp(-2\alpha r_{1a}-2\beta r_{1b}-2\beta r_{2a}-2\alpha r_{2b})\ , \tag{3.7}$$

where $k_1^0=\pi/R$. Substituting the Fourier transforms of (3.1) and (3.5), we obtain

$$\begin{aligned}&\int d^3r_1\int d^3r_2\int d^3r_a\int d^3r_b j_0^2(k_1^0r_1)j_0^2(k_1^0r_2)j_0^2(k_1^0r_a)j_0^2(k_1^0r_b)\\&\times\int d^3k_{ab}\int d^3k_{1a}\int d^3k_{1b}\int d^3k_{2a}\int d^3k_{2b}h(k_{ab},2\gamma,2\delta)g(k_{1a},2\alpha)g(k_{1b},2\beta)g(k_{2a},2\beta)g(k_{2b},2\alpha)\\&\times\exp[i\mathbf{k}_{ab}\cdot(\mathbf{r}_a-\mathbf{r}_b)+i\mathbf{k}_{1a}\cdot(\mathbf{r}_1-\mathbf{r}_a)-i\mathbf{k}_{1b}\cdot(\mathbf{r}_1-\mathbf{r}_b)+i\mathbf{k}_{2a}\cdot(\mathbf{r}_2-\mathbf{r}_a)-i\mathbf{k}_{2b}\cdot(\mathbf{r}_2-\mathbf{r}_b)]\ .\end{aligned} \tag{3.8}$$

Making use of the expansion of a plane wave in terms of spherical waves,[27] namely

$$e^{i\mathbf{k}\cdot\mathbf{r}}=\sum_{n=0}^{\infty}i^n(2n+1)j_n(kr)P_n(\cos\theta)\ , \tag{3.9}$$

where j_n and P_n are the spherical Bessel function and the Legendre polynomial of the nth order, respectively, and carrying out the integration with respect to the angular parts of r_1, r_2, r_a, r_b, k_{ab}, k_{1a}, k_{1b}, k_{2a}, and k_{2b}, we arrive at the expression

$$(4\pi)^{10}\int_0^R dr_a r_a^2 j_0^2(k_1^0 r_a)\int_0^R dr_b r_b^2 j_0^2(k_1^0 r_b)\int_0^R dr_1 r_1^2 j_0^2(k_1^0 r_1)\int_0^R dr_2 r_2^2 j_0^2(k_1^0 r_2)$$
$$\times\int_0^\infty dk_{ab}k_{ab}^2 h(k_{ab},2\gamma,2\delta)\int_0^\infty dk_{1a}k_{1a}^2 g(k_{1a},2\alpha)\int_0^\infty dk_{1b}k_{1b}^2 g(k_{1b},2\beta)$$
$$\times\int_0^\infty dk_{2a}k_{2a}^2 g(k_{2a},2\beta)\int_0^\infty dk_{2b}k_{2b}^2 g(k_{2b},2\alpha)$$
$$\times\sum_{l,m}\sum_{l',m'}\sum_{l'',m''}|(l',m',l'',m''|l,m)|^2 j_l(k_{ab}r_a)j_l(k_{ab}r_b)j_{l'}(k_{1a}r_1)j_{l'}(k_{1a}r_a)$$
$$\times j_{l'}(k_{1b}r_1)j_{l'}(k_{1b}r_b)j_{l''}(k_{2a}r_2)j_{l''}(k_{2a}r_a)j_{l''}(k_{2b}r_2)j_{l''}(k_{2b}r_b)\ . \quad (3.10)$$

Here $(l',m',l'',m''|l,m)$ and $(l,m|l',m',l'',m'')$ are the Gaunt coefficients,[28] defined by

$$(l',m',l'',m''|l,m)=\int d\Omega\, Y^*_{l',m'}(\Omega)Y^*_{l'',m''}(\Omega)Y_{l,m}(\Omega) \quad (3.11)$$

and

$$(l,m|l',m',l'',m'')=\int d\Omega\, Y^*_{l,m}(\Omega)Y_{l',m'}(\Omega)Y_{l'',m''}(\Omega)\ , \quad (3.12)$$

where the integration is over the solid angle. These coefficients have the following symmetry: $(l',m',l'',m''|l,m)=(l'',m'',l',m'|l,m)=(l,m|l',m',l'',m'')=(l,m|l'',m'',l',m')$. The expressions of the Gaunt coefficient are given in Appendix C. We can perform the k integration in (3.10) analytically as

$$\int_0^\infty dk\, k^2 g(k,\alpha)j_l(kr_i)j_l(kr_j)=G_l(r_i,r_j;\alpha) \quad (3.13)$$

and

$$\int_0^\infty dk\, k^2 h(k,\gamma,\delta)j_l(kr_i)j_l(kr_j)=H_l(r_i,r_j;\gamma,\delta)\ . \quad (3.14)$$

Similarly, in the calculation of the Coulomb energy, we need an integral defined by

$$\int_0^\infty dk\, k^2 f(k,\alpha)j_l(kr_i)j_l(kr_j)=F_l(r_i,r_j;\alpha)\ . \quad (3.15)$$

The explicit expressions of these functions are given in Appendix A. The final expression of (3.7) is obtained as

$$(4\pi)^{10}\int_0^R dr_a r_a^2 j_0^2(k_1^0 r_a)\int_0^R dr_b r_b^2 j_0^2(k_1^0 r_b)\int_0^R dr_1 r_1^2 j_0^2(k_1^0 r_1)\int_0^R dr_2 r_2^2 j_0^2(k_1^0 r_2)$$
$$\times\sum_{l,m}\sum_{l',m'}\sum_{l'',m''}|(l',m',l'',m''|l,m)|^2 H_l(r_a,r_b;2\gamma,2\delta)G_{l'}(r_1,r_a;2\alpha)G_{l'}(r_1,r_b;2\beta)G_{l''}(r_2,r_a;2\beta)G_{l''}(r_2,r_b;2\alpha)\ . \quad (3.16)$$

Then the normalization constant C_m is determined from

$$1=\langle\Phi_m|\Phi_m\rangle$$
$$=2C_m^2(4\pi)^{10}\int_0^R dr_a r_a^2 j_0^2(k_1^0 r_a)\int_0^R dr_b r_b^2 j_0^2(k_1^0 r_b)\int_0^R dr_1 r_1^2 j_0^2(k_1^0 r_1)$$
$$\times\int_0^R dr_2 r_2^2 j_0^2(k_1^0 r_2)\sum_{l,m}\sum_{l',m'}\sum_{l'',m''}|(l',m',l'',m''|l,m)|^2 H_l(r_a,r_b;2\gamma,2\delta)$$
$$\times[\,G_{l'}(r_1,r_a;2\alpha)G_{l'}(r_1,r_b;2\beta)G_{l''}(r_2,r_a;2\beta)G_{l''}(r_2,r_b;2\alpha)$$
$$+G_{l'}(r_1,r_a;\alpha+\beta)G_{l'}(r_1,r_b;\alpha+\beta)G_{l''}(r_2,r_a;\alpha+\beta)G_{l''}(r_2,r_b;\alpha+\beta)]\ . \quad (3.17)$$

B. Calculation of Coulomb energy

Now we calculate the Coulomb terms. From the symmetry of the variational wave function (2.3) with respect to the exchange of electrons and holes, it is obvious that

$$\left\langle\Phi_m\left|\frac{1}{|r_1-r_a|}\right|\Phi_m\right\rangle=\left\langle\Phi_m\left|\frac{1}{|r_2-r_a|}\right|\Phi_m\right\rangle=\left\langle\Phi_m\left|\frac{1}{|r_1-r_b|}\right|\Phi_m\right\rangle=\left\langle\Phi_m\left|\frac{1}{|r_2-r_b|}\right|\Phi_m\right\rangle\ . \quad (3.18)$$

Thus the six Coulomb integrals are reduced to three types of integral, namely

$$C_{1a}=\left\langle\Phi_m\left|\frac{e^2}{\epsilon_1|r_1-r_a|}\right|\Phi_m\right\rangle\ , \quad (3.19)$$

$$C_{ab}=\left\langle \Phi_m \left| \frac{e^2}{\epsilon_1 |r_a - r_b|} \right| \Phi_m \right\rangle , \tag{3.20}$$

$$C_{12}=\left\langle \Phi_m \left| \frac{e^2}{\epsilon_1 |r_1 - r_2|} \right| \Phi_m \right\rangle . \tag{3.21}$$

C_{ab} is given by e^2/ϵ_1 times the right-hand side of (3.17), replacing 2γ with $2\gamma-1$. Making use of the functions in (3.13)–(3.15), C_{1a} is calculated as

$$\begin{aligned} C_{1a}=&\frac{e^2(4\pi)^{10}C_m^2}{\epsilon_1}\int_0^R dr_a r_a^2 j_0^2(k_1^0 r_a)\int_0^R dr_b r_b^2 j_0^2(k_1^0 r_b)\int_0^R dr_1 r_1^2 j_0^2(k_1^0 r_1)\int_0^R dr_2 r_2^2 j_0^2(k_1^0 r_2) \\ &\times \sum_{l,m}\sum_{l',m'}\sum_{l'',m''} |(l',m',l'',m''|l,m)|^2 H_l(r_a,r_b;2\gamma,2\delta) \\ &\times [F_{l'}(r_1,r_a;2\alpha)G_{l'}(r_1,r_b;2\beta)G_{l''}(r_2,r_a;2\beta)G_{l''}(r_2,r_b;2\alpha)+F_{l'}(r_1,r_a;2\beta)G_{l'}(r_1,r_b;2\alpha)G_{l''}(r_2,r_a;2\alpha)G_{l''}(r_2,r_b;2\beta) \\ &+2F_{l'}(r_1,r_a;\alpha+\beta)G_{l'}(r_1,r_b;\alpha+\beta)G_{l''}(r_2,r_a;\alpha+\beta)G_{l''}(r_2,r_b;\alpha+\beta)] . \end{aligned} \tag{3.22}$$

To calculate the Coulomb energy C_{12} between two electrons, we employ the following expansion:[27]

$$\frac{1}{|r_1-r_2|}=\sum_{l=0}^{\infty}\frac{r_<^l}{r_>^{l+1}}P_l(\cos\theta_{12})=4\pi\sum_{l,m}\frac{r_<^l}{r_>^{l+1}}\frac{Y_{lm}^*(\Omega_1)Y_{lm}(\Omega_2)}{2l+1} , \tag{3.23}$$

where $r_>=\max(r_1,r_2)$, $r_<=\min(r_1,r_2)$, and Ω_1 (Ω_2) denotes the solid angle of r_1 (r_2). Then we have

$$\begin{aligned} C_{12}=&\frac{e^2(4\pi)^{11}C_m^2}{\epsilon_1}\int_0^R dr_a r_a^2 j_0^2(k_1^0 r_a)\int_0^R dr_b r_b^2 j_0^2(k_1^0 r_b)\int_0^R dr_1 r_1^2 j_0^2(k_1^0 r_1)\int_0^R dr_2 r_2^2 j_0^2(k_1^0 r_2) \\ &\times \sum_{n,p}\frac{r_<^n}{r_>^{n+1}}\frac{1}{2n+1}\sum_{l,m}\sum_{l',m'}\sum_{l'',m''}\sum_{\bar{l}',\bar{m}'}\sum_{\bar{l}'',\bar{m}''}(l',m',l'',m''|l,m)(l,m|\bar{l}',\bar{m}',\bar{l}'',\bar{m}'') \\ &\times(\bar{l}',\bar{m}'|l',m',n,p)(\bar{l}'',\bar{m}'',n,p|l'',m'')H_l(r_a,r_b;2\gamma,2\delta) \\ &\times[G_{l'}(r_1,r_a;2\alpha)G_{\bar{l}'}(r_1,r_b;2\beta)G_{l''}(r_2,r_a;2\beta)G_{\bar{l}''}(r_2,r_b;2\alpha) \\ &+G_{l'}(r_1,r_a;2\beta)G_{\bar{l}'}(r_1,r_b;2\alpha)G_{l''}(r_2,r_a;2\alpha)G_{\bar{l}''}(r_2,r_b;2\beta) \\ &+2G_{l'}(r_1,r_a;\alpha+\beta)G_{\bar{l}'}(r_1,r_b;\alpha+\beta)G_{l''}(r_2,r_a;\alpha+\beta)G_{\bar{l}''}(r_2,r_b;\alpha+\beta)] . \end{aligned} \tag{3.24}$$

C. Calculation of surface polarization energy

The details of calculation of the surface polarization energy are presented. From the symmetry of the variational wave function, we find

$$\langle \Phi_m | r_1^{2n} | \Phi_m \rangle = \langle \Phi_m | r_2^{2n} | \Phi_m \rangle , \tag{3.25}$$

$$\langle \Phi_m | r_a^{2n} | \Phi_m \rangle = \langle \Phi_m | r_b^{2n} | \Phi_m \rangle , \tag{3.26}$$

$$\begin{aligned} \langle \Phi_m | (r_1 r_a)^n P_n(\cos\theta_{1a}) | \Phi_m \rangle &= \langle \Phi_m | (r_1 r_b)^n P_n(\cos\theta_{1b}) | \Phi_m \rangle \\ &= \langle \Phi_m | (r_2 r_a)^n P_n(\cos\theta_{2a}) | \Phi_m \rangle = \langle \Phi_m | (r_2 r_b)^n P_n(\cos\theta_{2b}) | \Phi_m \rangle . \end{aligned} \tag{3.27}$$

Thus the surface polarization energy can be written in terms of five types of integrals, namely

$$S_{1a}^{(n)}=\langle \Phi_m | (r_1 r_a)^n P_n(\cos\theta_{1a}) | \Phi_m \rangle , \tag{3.28}$$

$$S_{12}^{(n)}=\langle \Phi_m | (r_1 r_2)^n P_n(\cos\theta_{12}) | \Phi_m \rangle , \tag{3.29}$$

$$S_{ab}^{(n)}=\langle \Phi_m | (r_a r_b)^n P_n(\cos\theta_{ab}) | \Phi_m \rangle , \tag{3.30}$$

$$S_{11}^{(n)}=\langle \Phi_m | (r_1)^{2n} | \Phi_m \rangle , \tag{3.31}$$

$$S_{aa}^{(n)}=\langle \Phi_m | (r_a)^{2n} | \Phi_m \rangle . \tag{3.32}$$

The integrals $S_{11}^{(n)}$ and $S_{aa}^{(n)}$ can be written similarly to (3.17). Expanding the Legendre polynomial in terms of spherical harmonics as[27]

$$P_n(\cos\theta_{12})=\frac{4\pi}{2n+1}\sum_{p=-n}^{n} Y_{np}(\Omega_1)Y_{np}^*(\Omega_2)\ , \tag{3.33}$$

we obtain essentially the same expression for $S_{12}^{(n)}$ as (3.24) except for the replacement of $r_<^n/r_>^{n+1}$ by $(r_1r_2)^n$. Through a similar procedure of calculation, $S_{1a}^{(n)}$ can be expressed as

$$\begin{aligned}S_{1a}^{(n)}=&\frac{(4\pi)^{11}C_m^2}{2n+1}\int_0^R dr_a r_a^2 j_0^2(k_1^0 r_a)\int_0^R dr_b r_b^2 j_0^2(k_1^0 r_b)\int_0^R dr_1 r_1^2 j_0^2(k_1^0 r_1)\int_0^R dr_2 r_2^2 j_0^2(k_1^0 r_2)\\ &\times(r_1r_a)^n\sum_p\sum_{l,m}\sum_{l',m'}\sum_{l'',m''}\sum_{\bar l,\bar m}(l',m',n,p|\bar l,\bar m)(\bar l,\bar m,l'',m''|l,m,n,p)(l,m|l',m',l'',m'')\\ &\times H_l(r_a,r_b;2\gamma,2\delta)[\,G_{\bar l}(r_1,r_a;2\alpha)G_{l'}(r_1,r_b;2\beta)G_{l''}(r_2,r_a;2\beta)G_{l''}(r_2,r_b;2\alpha)\\ &+G_{\bar l}(r_1,r_a;2\beta)G_{l'}(r_1,r_b;2\alpha)G_{l''}(r_2,r_a;2\alpha)G_{l''}(r_2,r_b;2\beta)\\ &+2G_{\bar l}(r_1,r_a;\alpha+\beta)G_{l'}(r_1,r_b;\alpha+\beta)\\ &\times G_{l''}(r_2,r_a;\alpha+\beta)G_{l''}(r_2,r_b;\alpha+\beta)]\ ,\end{aligned} \tag{3.34}$$

where $(l,m,\bar l,\bar m|l',m',l'',m'')$ is an integral of product of four spherical harmonics and its expression is given in Appendix C. In the same way, we find

$$\begin{aligned}S_{ab}^{(n)}=&\frac{(4\pi)^{11}C_m^2}{2n+1}\int_0^R dr_a r_a^2 j_0^2(k_1^0 r_a)\int_0^R dr_b r_b^2 j_0^2(k_1^0 r_b)\int_0^R dr_1 r_1^2 j_0^2(k_1^0 r_1)\int_0^R dr_2 r_2^2 j_0^2(k_1^0 r_2)\\ &\times(r_ar_b)^n\sum_p\sum_{l,m}\sum_{l',m'}\sum_{l'',m''}|(l',m',l'',m''|l,m,n,p)|^2 H_l(r_a,r_b;2\gamma,2\delta)\\ &\times[\,G_{l'}(r_1,r_a;2\alpha)G_{l'}(r_1,r_b;2\beta)G_{l''}(r_2,r_a;2\beta)G_{l''}(r_2,r_b;2\alpha)\\ &+G_{l'}(r_1,r_a;2\beta)G_{l'}(r_1,r_b;2\alpha)G_{l''}(r_2,r_a;2\alpha)G_{l''}(r_2,r_b;2\beta)\\ &+2G_{l'}(r_1,r_a;\alpha+\beta)G_{l'}(r_1,r_b;\alpha+\beta)G_{l''}(r_2,r_a;\alpha+\beta)G_{l''}(r_2,r_b;\alpha+\beta)]\ .\end{aligned} \tag{3.35}$$

D. Calculation of kinetic energy

Calculation of the kinetic energy is rather complicated and requires an efficient algorithm. We make full use of the vanishing property of the wave function at the particle surface and the Gauss formula. First of all, from the symmetry of the wave function Φ_m, we notice that

$$\langle\Phi_m|\nabla_1^2|\Phi_m\rangle=\langle\Phi_m|\nabla_2^2|\Phi_m\rangle,\quad \langle\Phi_m|\nabla_a^2|\Phi_m\rangle=\langle\Phi_m|\nabla_b^2|\Phi_m\rangle\ . \tag{3.36}$$

From the Gauss formula, we find that

$$\int d\tau\,\Phi_m\nabla_1^2\Phi_m=-\int d\tau(\nabla_1\Phi_m)^2,\quad \int d\tau\,\Phi_m\nabla_a^2\Phi_m=-\int d\tau(\nabla_a\Phi_m)^2\ , \tag{3.37}$$

where the integration $(d\tau)$ is carried out over r_a, r_b, r_1 and r_2. To reduce $(\nabla_1\Phi_m)^2$ into a tractable form, we factorize Φ_m as

$$\Phi_m=fgh\ , \tag{3.38}$$

with

$$f=j_0(k_1^0r_1)\ , \tag{3.39}$$

$$g=\exp(-\alpha r_{1a}-\beta r_{1b}-\beta r_{2a}-\alpha r_{2b})+\exp(-\beta r_{1a}-\alpha r_{1b}-\alpha r_{2a}-\beta r_{2b})\ , \tag{3.40}$$

$$h=j_0(k_1^0r_2)j_0(k_1^0r_a)j_0(k_1^0r_b)r_{ab}^{\gamma}e^{-\delta r_{ab}}\ . \tag{3.41}$$

Then we have

$$(\nabla_1\Phi_m)^2=[(\nabla_1f)^2g^2+2fg(\nabla_1f)(\nabla_1g)+f^2(\nabla_1g)^2]h^2=[(\nabla_1f)\nabla_1(fg^2)+f^2(\nabla_1g)^2]h^2\ , \tag{3.42}$$

and applying the Gauss formula to the first term, we find

$$\int d\tau(\nabla_1\Phi_m)^2=\int d\tau[-(\nabla_1^2f)fg^2+f^2(\nabla_1g)^2]h^2\ . \tag{3.43}$$

Noticing that $[\nabla_1^2+(k_1^0)^2]f=0$, we finally have

$$\langle\Phi_m|\nabla_1^2|\Phi_m\rangle=\int d\tau[-(k_1^0)^2f^2g^2-f^2(\nabla_1 g)^2]h^2 . \tag{3.44}$$

The first term is simply $-(k_1^0)^2$ times the normalization integral in (3.17). The second integrand is written as

$$\begin{aligned}f^2(\nabla_1 g)^2h^2=&\,j_0^2(k_1^0r_a)j_0^2(k_1^0r_b)j_0^2(k_1^0r_1)j_0^2(k_1^0r_2)r_{ab}^{2\gamma}e^{-2\delta r_{ab}}\\&\times\left[2\left[\alpha^2+\beta^2+2\alpha\beta\frac{\mathbf{r}_{1a}\cdot\mathbf{r}_{1b}}{r_{1a}r_{1b}}\right]\exp(-2\alpha r_{1a}-2\beta r_{1b}-2\beta r_{2a}-2\alpha r_{2b})\right.\\&\left.+2\left[2\alpha\beta+(\alpha^2+\beta^2)\frac{\mathbf{r}_{1a}\cdot\mathbf{r}_{1b}}{r_{1a}r_{1b}}\right]\exp[-(\alpha+\beta)(r_{1a}+r_{1b}+r_{2a}+r_{2b})]\right] .\end{aligned} \tag{3.45}$$

The integral of the first, second, and fourth terms in (3.45) can be expressed similarly to (3.7). To calculate the integral of the third term in (3.45), we notice that

$$4\alpha\beta\frac{\mathbf{r}_{1a}\cdot\mathbf{r}_{1b}}{r_{1a}r_{1b}}\exp(-2\alpha r_{1a}-2\beta r_{1b}-2\beta r_{2a}-2\alpha r_{2b})=\nabla_{1a}\cdot\nabla_{1b}\exp(-2\alpha r_{1a}-2\beta r_{1b}-2\beta r_{2a}-2\alpha r_{2b}) , \tag{3.46}$$

where r_{1a} and r_{1b} are regarded as independent variables. Introducing the Fourier transforms of (3.1) and (3.5), we can derive the expression

$$\begin{aligned}&\int d\tau j_0^2(k_1^0r_a)j_0^2(k_1^0r_b)j_0^2(k_1^0r_1)j_0^2(k_1^0r_2)r_{ab}^{2\gamma}e^{-2\delta r_{ab}}4\alpha\beta\frac{\mathbf{r}_{1a}\cdot\mathbf{r}_{1b}}{r_{1a}r_{1b}}\exp(-2\alpha r_{1a}-2\beta r_{1b}-2\beta r_{2a}-2\alpha r_{2b})\\&=\int d\tau j_0^2(k_1^0r_a)j_0^2(k_1^0r_b)j_0^2(k_1^0r_1)j_0^2(k_1^0r_2)\int d^3k_{ab}\int d^3k_{1a}\int d^3k_{1b}\int d^3k_{2a}\int d^3k_{2b}\\&\times h(k_{ab},2\gamma,2\delta)g(k_{1a},2\alpha)g(k_{1b},2\beta)g(k_{2a},2\beta)g(k_{2b},2\alpha)(\mathbf{k}_{1a}\cdot\mathbf{k}_{1b})\\&\times\exp[i\mathbf{k}_{ab}\cdot(\mathbf{r}_a-\mathbf{r}_b)+i\mathbf{k}_{1a}\cdot(\mathbf{r}_1-\mathbf{r}_a)-i\mathbf{k}_{1b}\cdot(\mathbf{r}_1-\mathbf{r}_b)+i\mathbf{k}_{2a}\cdot(\mathbf{r}_2-\mathbf{r}_a)-i\mathbf{k}_{2b}\cdot(\mathbf{r}_2-\mathbf{r}_b)] .\end{aligned} \tag{3.47}$$

Further introducing the expansion (3.9) and making use of the recurrence relation[27]

$$(2n+1)xP_n(x)=(n+1)P_{n+1}(x)+nP_{n-1}(x) , \tag{3.48}$$

we arrive at the expression

$$\begin{aligned}&(4\pi)^{10}C_m^2\int_0^R dr_a r_a^2 j_0^2(k_1^0r_a)\int_0^R dr_b r_b^2 j_0^2(k_1^0r_b)\int_0^R dr_1 r_1^2 j_0^2(k_1^0r_1)\int_0^R dr_2 r_2^2 j_0^2(k_1^0r_2)\\&\times\sum_{l,m}\sum_{l',m'}\sum_{l'',m''}|(l',m',l'',m''|l,m)|^2H_l(r_a,r_b;2\gamma,2\delta)G_{l''}(r_2,r_a;2\beta)G_{l''}(r_2,r_b;2\alpha)\\&\times\frac{1}{2l'+1}[l'G_{l'}^-(r_a,r_1;2\alpha)G_{l'}^-(r_b,r_1;2\beta)+(l'+1)G_{l'}^+(r_a,r_1;2\alpha)G_{l'}^+(r_b,r_1;2\beta)] ,\end{aligned} \tag{3.49}$$

where $G_l^{\pm}$ is defined by

$$G_l^{\pm}(r_i,r_j;\alpha)=\int_0^\infty dk\, k^3 g(k,\alpha)j_l(kr_i)j_{l\pm1}(kr_j) , \tag{3.50}$$

with $g(k,\alpha)$ given in (3.3) and its analytic expression is given in Appendix A. The integral of the fifth term in (3.45) can be calculated in a similar manner. These complete the calculation of $\langle\Phi_m|\nabla_1^2|\Phi_m\rangle$.

Now let us proceed to the calculation of $\langle\Phi_m|\nabla_a^2|\Phi_m\rangle$. Factorizing Φ_m as

$$\Phi_m=fghe , \tag{3.51}$$

with

$$f=j_0(k_1^0r_a) , \tag{3.52}$$

$$g=\exp(-\alpha r_{1a}-\beta r_{1b}-\beta r_{2a}-\alpha r_{2b})+\exp(-\beta r_{1a}-\alpha r_{1b}-\alpha r_{2a}-\beta r_{2b}) , \tag{3.53}$$

$$h=r_{ab}^{\gamma}e^{-\delta r_{ab}} , \tag{3.54}$$

$$e=j_0(k_1^0r_b)j_0(k_1^0r_1)j_0(k_1^0r_2) , \tag{3.55}$$

we can derive that

$$\int d\tau(\nabla_a\Phi_m)^2=\int d\tau[-(\nabla_a^2 f)fg^2h^2+f^2(\nabla_a g)^2h^2-f^2g^2h(\nabla_a^2h)-2(\nabla_a f\cdot\nabla_a h)fg^2h]e^2 . \tag{3.56}$$

Making use of the relations

$$[\nabla_a^2+(k_1^0)^2]f=0 \tag{3.57}$$

and

$$\nabla_a^2 h=\left[\frac{\gamma(\gamma+1)}{r_{ab}^2}-\frac{2\delta(\gamma+1)}{r_{ab}}+\delta^2\right]h\ , \tag{3.58}$$

we can perform the integration of the first and third terms in (3.56) in the same way as the normalization integral of (3.7). The calculation of the second term in (3.56) proceeds in a similar way to that of (3.45). For a typical term corresponding to (3.47), we obtain

$$\begin{aligned}&\int d\tau j_0^2(k_1^0 r_a)j_0^2(k_1^0 r_b)j_0^2(k_1^0 r_1)j_0^2(k_1^0 r_2)r_{ab}^{2\gamma}e^{-2\delta r_{ab}}4\alpha\beta\frac{\mathbf{r}_{a1}\cdot\mathbf{r}_{a2}}{r_{1a}r_{2a}}\exp(-2\alpha r_{1a}-2\beta r_{1b}-2\beta r_{2a}-2\alpha r_{2b})\\&=-\frac{(4\pi)^{11}}{3}\int_0^R dr_a r_a^2 j_0^2(k_1^0 r_a)\int_0^R dr_b r_b^2 j_0^2(k_1^0 r_b)\int_0^R dr_1 r_1^2 j_0^2(k_1^0 r_1)\int_0^R dr_2 r_2^2 j_0^2(k_1^0 r_2)\\&\times\sum_{l,m}\sum_{l',m'}\sum_{l'',m''}\sum_{l_1,m_1}\sum_{l_2,m_2}\sum_{\mu=-1}^{1} i^{l_1+l_2-l'-l''}(l',m',l'',m''|l,m)(l,m|l_1,m_1,l_2,m_2)\\&\qquad\times(l_1,m_1,1,\mu|l',m')(l_2,m_2|l'',m'',1,\mu)H_l(r_a,r_b;2\gamma,2\delta)\\&\qquad\times G_{l_1}^{(l'-l_1)}(r_1,r_a;2\alpha)G_{l_1}(r_1,r_b;2\beta)G_{l_2}^{(l''-l_2)}(r_2,r_a;2\beta)G_{l_2}(r_2,r_b;2\alpha)\ ,\end{aligned} \tag{3.59}$$

where $l'=l_1\pm1$ and $l''=l_2\pm1$ and the superscript $(l'-l_1)$ or $(l''-l_2)$ corresponds to $(\pm)$ in (3.50). In this way the second term in (3.56) can be calculated. The calculation of the fourth term in (3.56) is performed as follows. First of all, we have

$$\begin{aligned}-2(\nabla_a f\cdot\nabla_a h)fg^2he^2=&\,4k_1^0\frac{\mathbf{r}_a\cdot\mathbf{r}_{ab}}{r_a r_{ab}}\left[\frac{\gamma}{r_{ab}}-\delta\right]j_0(k_1^0 r_a)j_1(k_1^0 r_a)j_0^2(k_1^0 r_b)j_0^2(k_1^0 r_1)j_0^2(k_1^0 r_2)r_{ab}^{2\gamma}e^{-2\delta r_{ab}}\\&\times\{\exp(-2\alpha r_{1a}-2\beta r_{1b}-2\beta r_{2a}-2\alpha r_{2b})+\exp[-(\alpha+\beta)(r_{1a}+r_{1b}+r_{2a}+r_{2b})]\}\ .\end{aligned} \tag{3.60}$$

Noticing the relation

$$2\frac{\mathbf{r}_a\cdot\mathbf{r}_{ab}}{r_a r_{ab}}\left[\frac{\gamma}{r_{ab}}-\delta\right]r_{ab}^{2\gamma}e^{-2\delta r_{ab}}=\frac{\mathbf{r}_a}{r_a}\nabla_{ab}(r_{ab}^{2\gamma}e^{-2\delta r_{ab}})\ , \tag{3.61}$$

and introducing the Fourier transform of the exponential functions, we can rewrite the integral of the first term in the curly braces of (3.60) as

$$\begin{aligned}&2ik_1^0\int d\tau j_0(k_1^0 r_a)j_1(k_1^0 r_a)j_0^2(k_1^0 r_b)j_0^2(k_1^0 r_1)j_0^2(k_1^0 r_2)\int d^3k_{ab}\int d^3k_{1a}\int d^3k_{1b}\\&\qquad\times\int d^3k_{2a}\int d^3k_{2b}h(k_{ab},2\gamma,2\delta)g(k_{1a},2\alpha)g(k_{1b},2\beta)g(k_{2a},2\beta)g(k_{2b},2\alpha)\frac{\mathbf{r}_a\cdot\mathbf{k}_{ab}}{r_a}\\&\times\exp[i\mathbf{k}_{ab}\cdot(\mathbf{r}_a-\mathbf{r}_b)+i\mathbf{k}_{1a}\cdot(\mathbf{r}_1-\mathbf{r}_a)-i\mathbf{k}_{1b}\cdot(\mathbf{r}_1-\mathbf{r}_b)+i\mathbf{k}_{2a}\cdot(\mathbf{r}_2-\mathbf{r}_a)-i\mathbf{k}_{2b}\cdot(\mathbf{r}_2-\mathbf{r}_b)]\ .\end{aligned} \tag{3.62}$$

Substituting the expansion (3.9) for the plane wave and making use of the recurrence relations[27] of (3.48) and

$$j_l'(x)=[lj_{l-1}(x)-(l+1)j_{l+1}(x)]/(2l+1)\ , \tag{3.63}$$

we obtain the final expression

$$\begin{aligned}&2k_1^0(4\pi)^{10}\int_0^R dr_a r_a^2 j_0(k_1^0 r_a)j_1(k_1^0 r_a)\int_0^R dr_b r_b^2 j_0^2(k_1^0 r_b)\int_0^R dr_1 r_1^2 j_0^2(k_1^0 r_1)\int_0^R dr_2 r_2^2 j_0^2(k_1^0 r_2)\\&\qquad\times\sum_{l,m}\sum_{l',m'}\sum_{l'',m''}|(l',m',l'',m''|l,m)|^2 P_l(r_a,r_b;2\gamma,2\delta)\\&\qquad\times G_{l'}(r_1,r_a;2\alpha)G_{l'}(r_1,r_b;2\beta)G_{l''}(r_2,r_a;2\beta)G_{l''}(r_2,r_b;2\alpha)\ ,\end{aligned} \tag{3.64}$$

where P_l is defined by

$$P_l(r_a,r_b;2\gamma,2\delta)=\int_0^\infty dk\,k^3h(k,2\gamma,2\delta)j_l'(kr_a)j_l(kr_b)\ , \tag{3.65}$$

with $h(k,\gamma,\delta)$ given in (3.6) and its explicit expression is given in Appendix A. Here j_l' is the first derivative of j_l. The integral of the second term in the curly braces of (3.60) can be rewritten in a manner similar to (3.64).

Now the basic integrals appearing in the kinetic-energy terms are all reduced to numerically tractable forms. The expansion in terms of spherical harmonics in all the above expressions is carried out up to $l=10$ to assure sufficient accuracy.

IV. RESULTS AND DISCUSSION

The biexciton binding energy B_{XX} is defined by the difference between the biexciton energy E_{XX} and twice the exciton energy $2E_X$, namely

$$B_{XX}=2E_X-E_{XX} \ . \tag{4.1}$$

This binding energy is a function of the quantum-dot radius R, the electron-to-hole mass ratio m_e/m_h, and the dielectric constant ratio ϵ_1/ϵ_2 of the semiconductor material to the surrounding medium. The dependence of B_{XX} on the quantum-dot radius R is plotted in Fig. 1 for a few values of the electron-to-hole mass ratio m_e/m_h with a fixed value of ϵ_1/ϵ_2 (=4.0). In the following the units of energy and length will be taken as the effective exciton Rydberg (Ry) and the exciton Bohr radius (a_B), respectively, of the bulk semiconductor material. The binding energy increases as the radius is reduced and this increase is stronger for smaller electron-to-hole mass ratio. However, as the particle size is reduced further, the binding energy begins to decrease and eventually becomes negative. This implies that the exciton-exciton interaction becomes repulsive in a small-sized particle. In a small-sized particle the increase in the electron-electron and hole-hole Coulomb repulsion becomes predominant and cannot be compensated for by the deformation of the wave function for the four-particle relative motion. The dependence of B_{XX} on the quantum-dot radius is again plotted in Fig. 2 for a few values of the dielectric constant ratio ϵ_1/ϵ_2 with a fixed value of m_e/m_h (=0.2). The increase of the binding energy is stronger for a larger value of ϵ_1/ϵ_2. This is a manifestation of the dielectric confinement effect. The dependence of B_{XX} on the electron-to-hole mass ratio is given in Fig. 3 for a few values of the quantum-dot radius with a fixed value of ϵ_1/ϵ_2 (=4.0). The binding energy increases with decreasing m_e/m_h and takes a maximum value at the hydrogen limit ($m_e/m_h=0$) as in the case of bulk materials.[26] The increasing trend is stronger for smaller particle radius as a manifestation of the quantum confinement effect. In Fig. 4, the same dependence is plotted for a few values of the dielectric constant ratio ϵ_1/ϵ_2 with a fixed value of R/a_B (=1.0). It is again confirmed that the binding energy depends strongly on the dielectric constant ratio ϵ_1/ϵ_2.

In order to see more clearly the importance of the dielectric confinement effect in enhancing the biexciton binding energy, we plot B_{XX} as a function of the dielectric constant ratio ϵ_1/ϵ_2 in Fig. 5 for several values of R/a_B with a fixed value of m_e/m_h (=0.2). The binding energy increases with increasing ϵ_1/ϵ_2 and the increase is prominent for smaller quantum-dot size. In Fig. 6, the same dependence is plotted for several values of the electron-to-hole mass ratio m_e/m_h with a fixed value of R/a_B (=1.0). In this case also, the strong dependence of B_{XX} on ϵ_1/ϵ_2 is demonstrated.

Finally, the variational parameters α, β, and δ, which minimize the biexciton energy, will be plotted. In the variational calculation, the parameter γ is fixed to be unity for simplicity of numerical calculation because the numerical algorithm becomes too time consuming for general real numbers of γ. However, we confirmed that this restriction does not bring about any serious error in estimating the binding energy and the oscillator strength of the biexciton state. In Fig. 7 these parameters are plotted as a function of the dielectric constant ratio ϵ_1/ϵ_2 with fixed values of R/a_B (=1.0) and m_e/m_h (=0.2). Here these parameters are scaled by k_1^0, namely α/k_1^0, β/k_1^0, and δ/k_1^0 are plotted. It is to be noted that the parameter

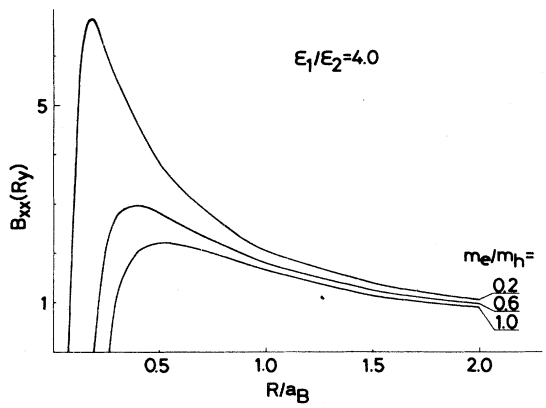

FIG. 1. Dependence of the biexciton binding energy B_{XX} on the quantum-dot radius R normalized by the bulk exciton Bohr radius a_B is plotted for a few values of the electron-to-hole mass ratio m_e/m_h with a fixed value of ϵ_1/ϵ_2 (=4.0).

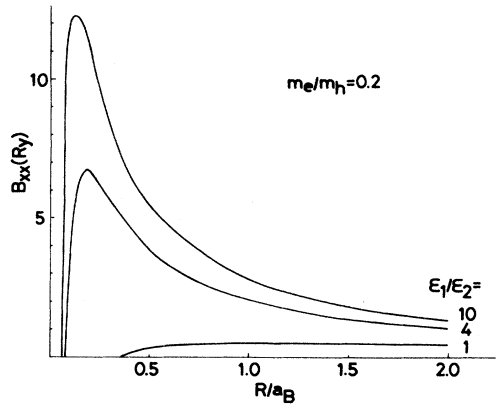

FIG. 2. Dependence of the biexciton binding energy B_{XX} on the quantum-dot radius R normalized by the bulk exciton Bohr radius a_B is plotted for a few values of the dielectric constant ratio ϵ_1/ϵ_2 with a fixed value of m_e/m_h (=0.2).

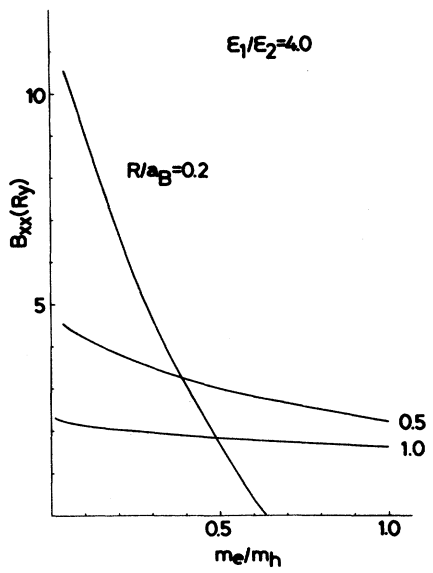

FIG. 3. Dependence of the biexciton binding energy B_{XX} on the electron-to-hole mass ratio m_e/m_h is plotted for a few values of the quantum-dot radius R/a_B with a fixed value of ϵ_1/ϵ_2 (=4.0).

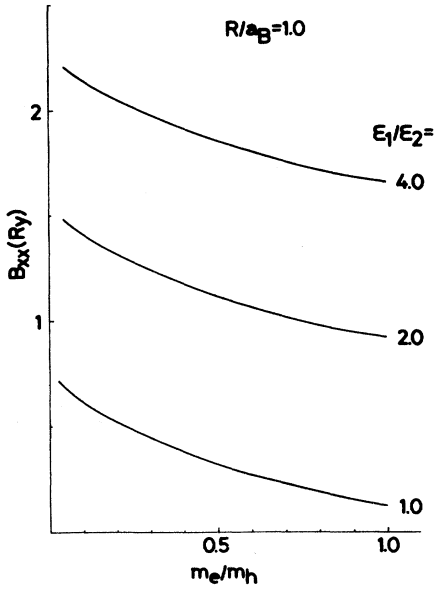

FIG. 4. Dependence of the biexciton binding energy B_{XX} on the electron-to-hole mass ratio m_e/m_h is plotted for a few values of the dielectric constant ratio ϵ_1/ϵ_2 with a fixed value of R/a_B (=1.0).

β takes negative values. The parameter δ shows a rather large change compared to α and β. This implies that the hole-hole separation is affected much by the change of the dielectric constant ratio due to the enhanced Coulomb interaction, while the electron-hole relative motion shows little change. In Fig. 8 the variational parameters are plotted as a function of the electron-to-hole mass ratio m_e/m_h with fixed values of R/a_B (=1.0) and ϵ_1/ϵ_2 (=4.0). As the hole mass becomes lighter, the hole kinetic energy increases and the hole-hole relative motion becomes extended. At the same time the electron-hole relative motion is also affected.

V. OSCILLATOR STRENGTH OF TRANSITION FROM EXCITON TO BIEXCITON STATES

Now that the variational wave function of the lowest biexciton state has been determined and the exciton wave function in a quantum dot is already obtained in the previous paper,[9] we can calculate the oscillator strength of transition from exciton to biexciton states. This oscillator strength will be denoted by f_{XX} and that of the excitonic transition by f_X, respectively. These are given by

$$f_{XX}=\frac{2}{m_0\hbar\omega_{XX\text{-}X}}|\langle XX|p|X\rangle|^2 , \tag{5.1}$$

$$f_X=\frac{2}{m_0\hbar\omega_X}|\langle X|p|0\rangle|^2 , \tag{5.2}$$

where $|X\rangle$ and $|XX\rangle$ denote, respectively, the exciton and the biexciton states, m_0 is the free-electron mass, p is the momentum operator, and $\hbar\omega_X$ and $\hbar\omega_{XX\text{-}X}$ are the exciton energy and the transition energy from exciton to biexciton states, respectively. The exciton and biexciton state wave functions including explicitly the spin structure can be written as

$$|X\rangle=\frac{C_e}{\sqrt{2}}\sum_{r_e,r_h}\Phi_e(r_e,r_h)(a^\dagger_{cr_e\alpha}a_{vr_h\alpha}+a^\dagger_{cr_e\beta}a_{vr_h\beta})|0\rangle , \tag{5.3}$$

$$|XX\rangle=\frac{C_m}{4}\sum_{r_1,r_2,r_a,r_b}\Phi_m(r_1,r_2,r_a,r_b)(a^\dagger_{cr_1\alpha}a^\dagger_{cr_2\beta}-a^\dagger_{cr_1\beta}a^\dagger_{cr_2\alpha})(a_{vr_a\alpha}a_{vr_b\beta}-a_{vr_a\beta}a_{vr_b\alpha})|0\rangle , \tag{5.4}$$

where the second-quantized form in the Wannier representation is employed, α (β) represents the spin-up (-down) state, Φ_e and C_e are the exciton wave function and its normalization constant, respectively, and $|0\rangle$ denotes the ground state of the crystal. Then the momentum matrix element is calculated as

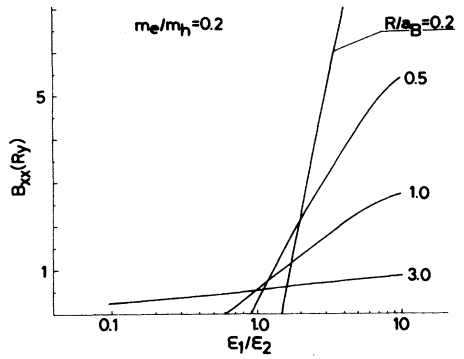

FIG. 5. Dependence of the biexciton binding energy B_{XX} on the dielectric constant ratio ϵ_1/ϵ_2 is plotted for several values of R/a_B with a fixed value of m_e/m_h (=0.2).

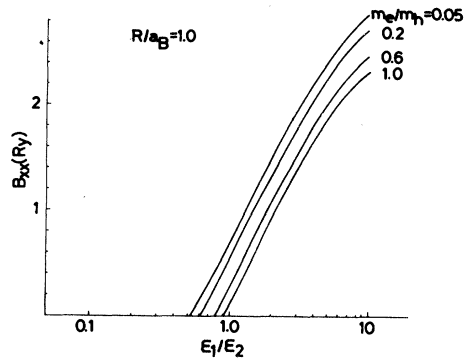

FIG. 6. Dependence of the biexciton binding energy B_{XX} on the dielectric constant ratio ϵ_1/ϵ_2 is plotted for several values of m_e/m_h with a fixed value of R/a_B (=1.0).

$$\langle XX|p|X\rangle = \sqrt{2}C_e C_m m_{cv} \sum_{r_1,r_2,r_b} \Phi_m(r_1,r_2,r_1,r_b)\Phi_e(r_2,r_b) , \tag{5.5}$$

where $m_{cv}=\langle cr|p|vr\rangle$ is the momentum matrix element between atomic Wannier orbitals. This is written more explicitly as

$$\sqrt{2}m_{cv}\frac{C_m C_e}{(v_0)^3}\int d^3r_1 \int d^3r_2 \int d^3r_b j_0^2(k_1^0 r_1) j_0^2(k_1^0 r_2) j_0^2(k_1^0 r_b) r_{1b}^{\gamma} e^{-\delta r_{1b}}$$

$$\times\{\exp[-\alpha r_{1b}-\alpha r_{12}-(\beta+\alpha_e)r_{2b}]+\exp[-\beta r_{1b}-\beta r_{12}-(\alpha+\alpha_e)r_{2b}]\} , \tag{5.6}$$

where v_0 is the volume of the unit cell, α_e is the inverse exciton Bohr radius in a quantum dot, and α, β, γ, and δ are

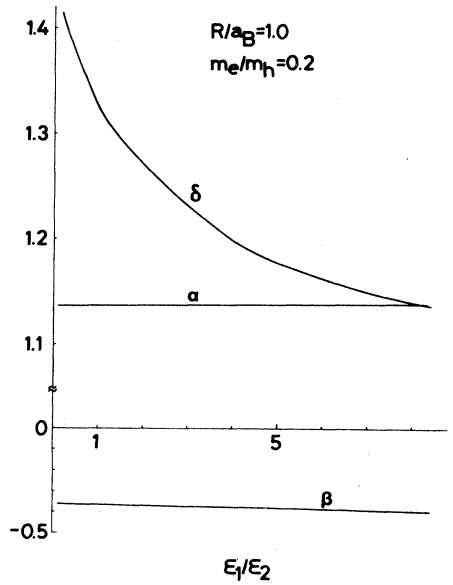

FIG. 7. The variational parameters α, β, and δ scaled by k_1^0 are plotted as a function of the dielectric constant ratio ϵ_1/ϵ_2 with fixed values of R/a_B (=1.0) and m_e/m_h (=0.2).

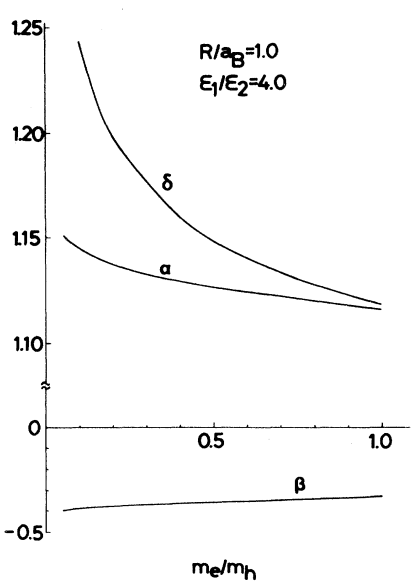

FIG. 8. The variational parameters α, β, and δ scaled by k_1^0 are plotted as a function of the electron-to-hole mass ratio m_e/m_h with fixed values of R/a_B (=1.0) and ϵ_1/ϵ_2 (=4.0).

the variational parameters concerning the biexciton state. A typical integral in (5.6) can be calculated as

$$\int d^3r_1 \int d^3r_2 \int d^3r_b j_0^2(k_1^0 r_1) j_0^2(k_1^0 r_2) j_0^2(k_1^0 r_b) r_{1b}^{\gamma} e^{-\delta r_{1b} - \alpha r_{12} - \beta r_{2b}}$$
$$= (4\pi)^6 \int_0^R dr_1 r_1^2 \int_0^R dr_2 r_2^2 \int_0^R dr_b r_b^2 j_0^2(k_1^0 r_1) j_0^2(k_1^0 r_2) j_0^2(k_1^0 r_b) \sum_{l=0}^{\infty} (2l+1) H_l(r_1, r_b; \gamma, \delta) G_l(r_1, r_2; \alpha) G_l(r_2, r_b; \beta) . \tag{5.7}$$

On the other hand, the momentum matrix element of the exciton transition is calculated as

$$\langle X|p|0\rangle = m_{cv}\pi^2 \left[\frac{1}{2\pi a I(a)} \right]^{1/2} , \tag{5.8}$$

where $a = 2\alpha_e / k_1^0$ and

$$I(a) = \int_0^{\infty} dk \frac{1}{(k^2+a^2)^2} \{ \mathrm{Si}(k\pi) - \tfrac{1}{2}[\mathrm{Si}((k+2)\pi) + \mathrm{sgn}(k-2)\mathrm{Si}(|k-2|\pi)] \}^2 , \tag{5.9}$$

where Si is the sine integral function. The biexciton oscillator strength f_{XX} will be normalized by the oscillator strength f_0 of the band-to-band transition given by

$$f_0 = \frac{2}{m_0 E_g} |m_{cv}|^2 , \tag{5.10}$$

where E_g is the band-gap energy. In the following, however, we will assume $\hbar\omega_{XX\text{-}X} \cong \hbar\omega_X \cong E_g$ and will plot essentially the ratios of the squared momentum matrix elements as

$$f_{XX}/f_0 \cong |\langle XX|p|X\rangle|^2 / m_{cv}^2 , \tag{5.11}$$

$$f_X/f_0 \cong |\langle X|p|0\rangle|^2 / m_{cv}^2 . \tag{5.12}$$

In Fig. 9 the normalized oscillator strength f_{XX}/f_0 is plotted as a function of the quantum-dot radius for a few values of m_e/m_h with a fixed value of ϵ_1/ϵ_2 (=4.0). The oscillator strength increases with increasing quantum-dot radius as in the case of excitonic transition.[9] This is because the number of unit cells available for coherent excitonic or biexcitonic polarization increases with the particle size. The increasing trend of the oscillator strength is stronger for smaller values of m_e/m_h. In the limit of vanishing quantum-dot radius, the oscillator strength should go to zero because there is no unit cell sustaining the transition dipole moment. Here, however, the plotted quantities are essentially the ratios of the squared momentum matrix elements as shown in (5.11) and (5.12) and we have a finite value (=2.0) of f_{XX}/f_0 in the limit of $R \to 0$. Actually, the subband energies and $\omega_{XX\text{-}X}$ become infinite, resulting in the vanishing f_{XX}, according to (5.1). Furthermore, it is interesting to note that in the limit of $R \to 0$, we have

$$|\langle XX|p|X\rangle|^2 / |\langle X|p|0\rangle|^2 = 1 . \tag{5.13}$$

This implies that the two excitons composing a biexciton become uncorrelated in a small-sized particle because the kinetic energy dominates over the Coulomb correlation energy.

In order to look at the effect of the dielectric confinement, the dependence of f_{XX} on R is plotted in Fig. 10 for a few values of ϵ_1/ϵ_2 with a fixed value of m_e/m_h (=0.2). The difference due to the change of the dielectric constant ratio is rather small. In Fig. 11 f_{XX} is plotted as a function of m_e/m_h for several values of the quantum-dot radius R with a fixed value of ϵ_1/ϵ_2 (=4.0). The dependence on m_e/m_h is rather weak compared to that on R. The same dependence is plotted in Fig. 12 in

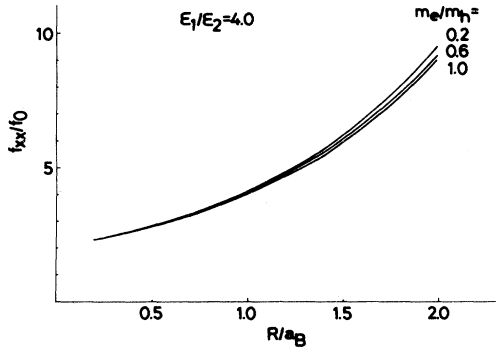

FIG. 9. Dependence of the normalized biexciton oscillator strength f_{XX}/f_0 on the quantum-dot radius R/a_B is plotted for a few values of m_e/m_h with a fixed value of ϵ_1/ϵ_2 (=4.0).

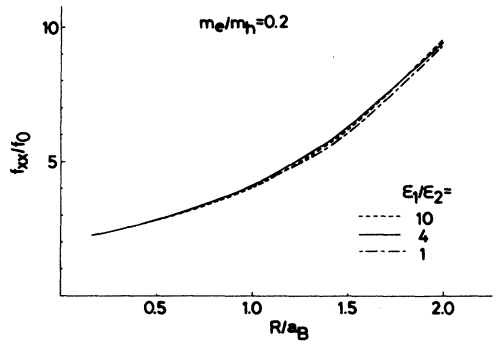

FIG. 10. Dependence of the normalized biexciton oscillator strength f_{XX}/f_0 on the quantum-dot radius R/a_B is plotted for a few values of ϵ_1/ϵ_2 with a fixed value of m_e/m_h (=0.2).

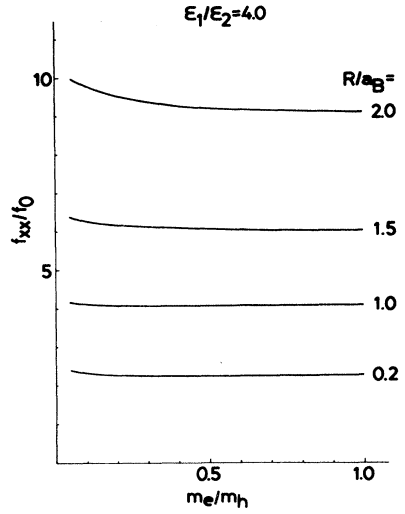

FIG. 11. Dependence of the normalized biexciton oscillator strength f_{XX}/f_0 on the electron-to-hole mass ratio m_e/m_h is plotted for several values of R/a_B with a fixed value of ϵ_1/ϵ_2 (=4.0).

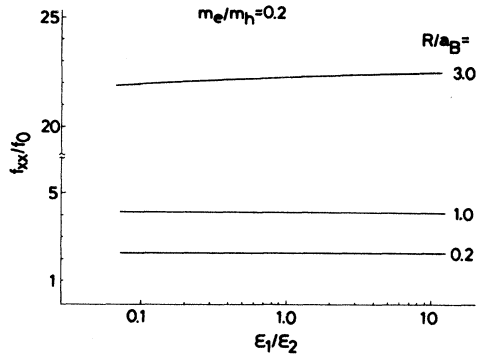

FIG. 13. Dependence of the normalized biexciton oscillator strength f_{XX}/f_0 on the dielectric constant ratio ϵ_1/ϵ_2 is plotted for a few values of R/a_B with a fixed value of m_e/m_h (=0.2).

an expanded scale for a few values of ϵ_1/ϵ_2 with a fixed value of R/a_B (=1.0). In this case also the dependence on ϵ_1/ϵ_2 is not very strong.

In order to see more clearly the dielectric confinement effect, the oscillator strength f_{XX} is plotted as a function of ϵ_1/ϵ_2 with a fixed value of m_e/m_h (=0.2) in Fig. 13 and with a fixed value of R/a_B (=1.0) in Fig. 14, respectively. The dependence on ϵ_1/ϵ_2 is rather weak in either case. Furthermore, in Fig. 14, f_{XX} begins to decrease when ϵ_1/ϵ_2 exceeds a certain value. In order to inspect the reason for this rather weak dependence, we plot the normalized exciton oscillator strength f_X/f_0 and the ratio of the oscillator strength of the biexciton state to that of the exciton state f_{XX}/f_X in Fig. 15 as a function of ϵ_1/ϵ_2 with fixed values of R/a_B (=1.0) and m_e/m_h (=0.2). It is found that f_X/f_0 and f_{XX}/f_X have opposite dependence on ϵ_1/ϵ_2, and that as a product of both factors, f_{XX}/f_0 is almost constant. The increase in f_X/f_0 with increasing ϵ_1/ϵ_2 is a consequence of dielectric confinement, which enhances the electron-hole Coulomb binding. The extent of electron-hole relative motion shrinks and the spatial overlap between an electron and a hole increases, leading to the increase in f_X. The oscillator strength f_{XX} is associated with the process of creating another exciton to form a biexciton when an exciton is already present. It is proportional partly to the spatial extent of the exciton-exciton relative motion in the biexciton state. The hole-hole relative motion, which gives a measure of the exciton-exciton relative motion, becomes extended with increasing ϵ_1/ϵ_2, as seen from δ in Fig. 7. However, since all particles are confined within a microcrystallite, the spatial extent of the exciton-exciton relative motion has an upper limit and is not

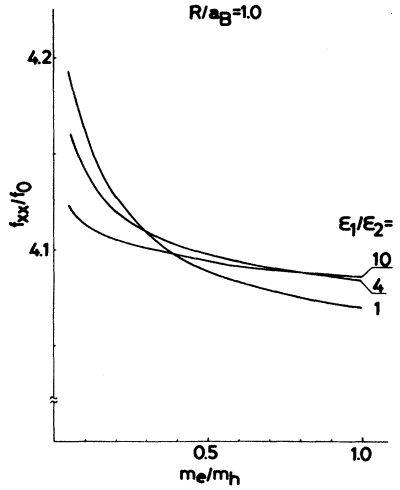

FIG. 12. Dependence of the normalized biexciton oscillator strength f_{XX}/f_0 on the electron-to-hole mass ratio m_e/m_h is plotted for a few values of ϵ_1/ϵ_2 with a fixed value of R/a_B (=1.0). Note that the vertical scale is expanded compared to that in Fig. 11.

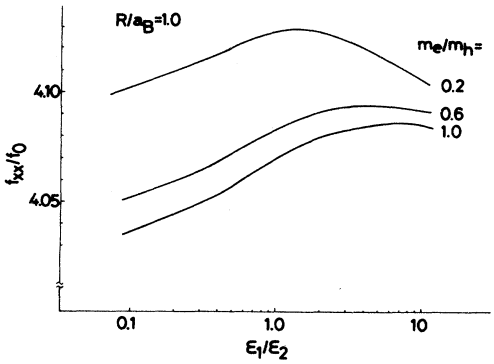

FIG. 14. Dependence of the normalized biexciton oscillator strength f_{XX}/f_0 on the dielectric constant ratio ϵ_1/ϵ_2 is plotted for a few values of m_e/m_h with a fixed value of R/a_B (=1.0). Note that the vertical scale is expanded compared to that in Fig. 13.

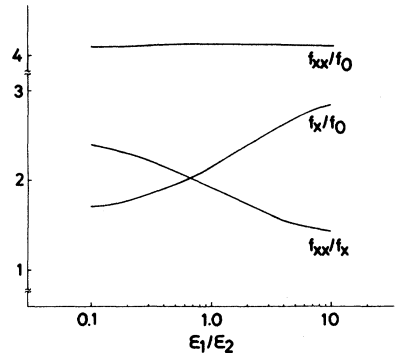

FIG. 15. The normalized exciton oscillator strength f_X/f_0 and the ratio of oscillator strength of the biexciton state to that of the exciton state f_{XX}/f_X are plotted as a function of the dielectric constant ratio ϵ_1/ϵ_2 with fixed values of R/a_B (=1.0) and m_e/m_h (=0.2).

strongly dependent on the dielectric constant ratio ϵ_1/ϵ_2. This explains the weak dependence of f_{XX}/f_0 on ϵ_1/ϵ_2. Thus the dielectric confinement is not very effective in enhancing the oscillator strength f_{XX}. However, since the oscillator strength for the two-photon generation of a biexciton state is proportional to the product $f_{XX}f_X$, the biexciton resonance can be enhanced by the dielectric confinement effect, namely for a large value of the dielectric constant ratio ϵ_1/ϵ_2.

Thus the large oscillator strength of the biexciton resonance is demonstrated in a semiconductor quantum dot. It is predicted that in order to obtain a large oscillator strength, it is favorable to choose a small value of m_e/m_h, a large value of R, and an optimum value of ϵ_1/ϵ_2. Since, as mentioned before, our calculation is carried out for the strong-confinement regime, in which the subband energy spacings of both electrons and holes are larger than the Coulomb binding energy, the argument of the increase of f_X and f_{XX} with the particle radius should be restricted within this regime. Actually, the magnitude of oscillator strength is determined by the coherence volume of excitonic or biexcitonic polarization[29,30] and in turn the coherence volume is limited by scattering by phonons and by defects or impurities. Thus there would exist an optimum particle size for obtaining a maximum oscillator strength.

VI. NONLINEAR OPTICAL PROPERTIES AND TWO-PHOTON ABSORPTION OF THE BIEXCITON

As discussed in the preceding section, the two-photon excitation of the biexciton state has a large oscillator strength. Accordingly, the optical nonlinearity via the biexcitonic state is expected to be enhanced. At the same time, this nonlinearity arises from the two-photon coherence instead of the population saturation of the excitonic state and thus it holds a promise of very fast optical response.

A. Nonlinear optical properties of the biexciton

In this subsection the optical nonlinearity via the exciton and biexciton states will be discussed on the basis of a three-level model. Hereafter, the ground state will be denoted by g, the excitonic state by e, and the biexciton state by b, respectively. Through the perturbation expansion up to the third order as given in Appendix E, we obtain the third-order nonlinear optical susceptibility $\chi^{(3)}$ as

$$\begin{aligned}\chi^{(3)}(2\omega_1-\omega_2;-\omega_1,-\omega_1,\omega_2)=&-\frac{i|\mu_{eg}|^4}{2\hbar^3}\frac{1}{i(\omega_{eg}-2\omega_1+\omega_2)+\gamma_{eg}}\frac{1}{i(\omega_2-\omega_1)+\gamma_{\parallel}^e}\\&\times\left[\frac{1}{i(\omega_{eg}-\omega_1)+\gamma_{eg}}+\frac{1}{i(\omega_2-\omega_{eg})+\gamma_{eg}}\right]\\&+\frac{i|\mu_{eg}|^2|\mu_{be}|^2}{4\hbar^3}\frac{1}{i(\omega_{be}-2\omega_1+\omega_2)+\gamma_{be}}\frac{1}{i(\omega_2-\omega_1)+\gamma_{\parallel}^e}\\&\times\left[\frac{1}{i(\omega_{eg}-\omega_1)+\gamma_{eg}}+\frac{1}{i(\omega_2-\omega_{eg})+\gamma_{eg}}\right]\\&-\frac{i|\mu_{eg}|^2|\mu_{be}|^2}{4\hbar^3}\frac{1}{i(\omega_{eg}-2\omega_1+\omega_2)+\gamma_{eg}}\frac{1}{i(\omega_{bg}-2\omega_1)+\gamma_{bg}}\frac{1}{i(\omega_{eg}-\omega_1)+\gamma_{eg}}\\&+\frac{i|\mu_{eg}|^2|\mu_{be}|^2}{4\hbar^3}\frac{1}{i(\omega_{be}-2\omega_1+\omega_2)+\gamma_{be}}\frac{1}{i(\omega_{bg}-2\omega_1)+\gamma_{bg}}\frac{1}{i(\omega_{eg}-\omega_1)+\gamma_{eg}},\end{aligned}\tag{6.1}$$

where $\hbar\omega_{ij}$, μ_{ij}, and γ_{ij} denote the energy difference, the transition dipole moment between i and j levels, and the dephasing rate of the transition dipole moment, respectively, and $\gamma_{\parallel}^e$ ($\gamma_{\parallel}^b$) is the population decay rate of the exciton (biexciton) state. The transition dipole moment is related to the oscillator strength as

$$\mu_{ij}^2=\frac{\hbar e^2}{2m_0\omega_{ij}}f_{ij}\ .\tag{6.2}$$

The first two terms in (6.1) arise from the saturation of excitonic population, whereas the remaining two terms arise from the nonlinearity via the two-photon coherence

of the biexciton state. In order to see the two-photon resonance with respect to the biexciton state, we introduce the off-resonance Δ, defined by

$$2\hbar\Delta=\hbar(2\omega_1-\omega_{bg}) . \tag{6.3}$$

Then other off resonances are given by

$$\hbar(\omega_{eg}-\omega_1)=B_{XX}/2-\hbar\Delta , \tag{6.4}$$

$$\hbar(\omega_{be}-\omega_1)=-B_{XX}/2-\hbar\Delta , \tag{6.5}$$

where B_{XX} is the biexciton binding energy given in (4.1). Thus the one-photon resonance appears at $\hbar\Delta=\pm B_{XX}/2$. In the following we consider the degenerate case, i.e., $\omega_1=\omega_2=\omega$.

In order to see the typical behaviors of the third-order susceptibility $\chi^{(3)}$, we scale all the off-resonance energies and the relaxation constants in terms of γ_{eg}, and choose the following typical values:

$$\gamma_{be}=\gamma_{eg},\quad \gamma_{bg}/\gamma_{eg}=0.1,1.0,\quad \gamma_{\parallel}^{e}/\gamma_{eg}=0.1 ,$$
$$|\mu_{be}|^2=|\mu_{eg}|^2,\quad B_{XX}/\hbar\gamma_{eg}=5.0 . \tag{6.6}$$

The frequency dispersion of $\chi^{(3)}$ for $\gamma_{bg}/\gamma_{eg}=0.1$ is shown in Fig. 16, which shows a resonance at the two-photon transition ($\Delta=0$) and two resonances at the one-photon transition ($\hbar\Delta=\pm B_{XX}/2$) corresponding to $\omega=\omega_{eg}$ and ω_{be}. It is interesting to note that the frequency dispersion at the two-photon resonance is opposite to that at the one-photon resonance ($\hbar\Delta=B_{XX}/2$). The imaginary part of $\chi^{(3)}$ at the two-photon resonance is positive and the real part changes its sign from negative to positive when the frequency is scanned from above, whereas the imaginary part of $\chi^{(3)}$ at the one-photon resonance is negative and the real part changes its sign from negative to positive when the frequency is scanned from below. These features of frequency dispersion can be understood qualitatively from (6.1). The frequency dispersion around the one-photon resonance at $\omega=\omega_{eg}$ is determined dominantly by the first term of (6.1) and can be written as

$$-\frac{i|\mu_{eg}|^4}{2\hbar^3\gamma_{\parallel}^{e}}\frac{2\gamma_{eg}}{(\omega-\omega_{eg})^2+\gamma_{eg}^2}\frac{1}{i(\omega_{eg}-\omega)+\gamma_{eg}} . \tag{6.7}$$

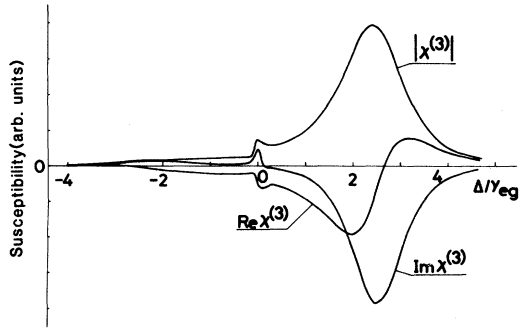

FIG. 16. Frequency dispersion of $\chi^{(3)}$. The parameters are given in the text. $\Delta=0$ corresponds to the two-photon resonance with the biexciton state and $\Delta=\pm B_{XX}/(2\hbar)$ ($=\pm 2.5\gamma_{eg}$) to the one-photon resonances, respectively.

Similarly, the frequency dispersion around another one-photon resonance at $\omega=\omega_{be}$ is contributed mainly by the second term of (6.1) and is approximated as

$$\frac{i|\mu_{eg}|^2|\mu_{be}|^2}{4\hbar^3\gamma_{\parallel}^{e}}\frac{2\gamma_{eg}}{(\omega-\omega_{eg})^2+\gamma_{eg}^2}\frac{1}{i(\omega_{be}-\omega)+\gamma_{be}} . \tag{6.8}$$

On the other hand, the frequency dispersion around the two-photon resonance at $2\omega=\omega_{bg}$ is determined by the third and fourth terms of (6.1) and can be approximated as

$$\frac{i|\mu_{eg}|^2|\mu_{be}|^2}{4\hbar^3}\left[\frac{1}{(B_{XX}/2\hbar)^2+\gamma_{eg}^2}-\frac{1}{(iB_{XX}/2\hbar+\gamma_{eg})^2}\right]\times\frac{1}{i(\omega_{bg}-2\omega)+\gamma_{bg}}$$
$$\cong\frac{i2|\mu_{eg}|^2|\mu_{be}|^2}{\hbar B_{XX}^2}\frac{1}{i(\omega_{bg}-2\omega)+\gamma_{bg}} , \tag{6.9}$$

where we assumed that $B_{XX}/\hbar\gg\gamma_{eg}$ and $\gamma_{be}\cong\gamma_{eg}$. From the sign of prefactors in front of the last complex Lorentzian factors in (6.7)–(6.9), it is seen that the frequency dispersion around the resonance at $\omega=\omega_{eg}$ is opposite to those around the resonances at $\omega=\omega_{be}$ and $2\omega=\omega_{bg}$. This feature is independent of the sign of the biexciton binding energy B_{XX}. The only difference due to the change of sign of B_{XX} appears in the order among three resonances on the frequency axis. In the case of positive B_{XX}, we have $\omega_{be}<\omega_{bg}/2<\omega_{eg}$, whereas for the case of negative B_{XX}, i.e., when the exciton-exciton interaction is repulsive, we have $\omega_{eg}<\omega_{bg}/2<\omega_{be}$. The schematic frequency dispersions around these resonances are plotted in Fig. 17.

The two-photon resonance is sensitive to the value of γ_{bg}. In the case of $\gamma_{bg}/\gamma_{eg}=1.0$, although not shown here, the two-photon resonance at $\Delta=0$ is smeared out by the broad background of the one-photon resonance at $\hbar\Delta=B_{XX}/2$, while the other parts of the frequency dispersion are almost identical to Fig. 16.

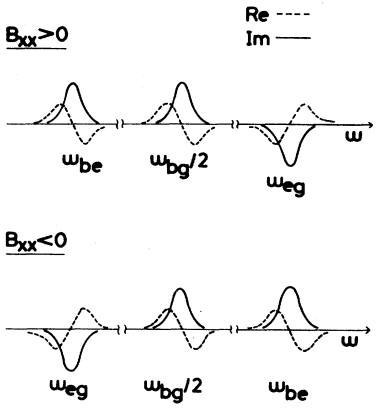

FIG. 17. Schematic representation of frequency dispersion of $\chi^{(3)}$ around the one- and two-photon resonances for positive and negative values of the biexciton binding energy B_{XX}. The real (imaginary) part is shown by a dashed (solid) line.

For the absorptive optical nonlinearity, the most appropriate figure of merit representing the efficiency of optical nonlinearity is $\chi^{(3)}$ divided by the product of the absorption coefficient α and the exciton (or photocarrier) lifetime τ. Denoting the incident power density and the number density of photoexcited carriers by I and N, respectively, the nonlinear change of α is related to the imaginary part of $\chi^{(3)}$ as

$$\alpha=\alpha_0+\alpha_2 I=\alpha_0+\sigma N \ , \tag{6.10}$$

$$\alpha_2=\frac{32\pi^2\omega}{\epsilon_0 c^2}\mathrm{Im}\chi^{(3)} \ , \tag{6.11}$$

$$\sigma=\frac{\hbar\omega}{\alpha_0\tau}\alpha_2 \ . \tag{6.12}$$

In the same way, the associated change of the refractive index n is related to the real part of $\chi^{(3)}$ as

$$n=n_0+n_2 I=n_0+\eta N \ , \tag{6.13}$$

$$n_2=\frac{16\pi^2}{\epsilon_0 c}\mathrm{Re}\chi^{(3)} \ , \tag{6.14}$$

$$\eta=\frac{\hbar\omega}{\alpha_0\tau}n_2 \ . \tag{6.15}$$

Here σ and η represent, respectively, the change of α and n per one electron-hole pair or an exciton in a unit volume, and have dimensions of area and volume. The derivation of these relations is given in Appendix F. Thus $\chi^{(3)}/\alpha_0\tau$ is a fundamental quantity describing the efficiency of absorptive optical nonlinearity. The carrier lifetime τ is in general dependent on the carrier energy. Hereafter, however, we ignore the energy dependence of τ and calculate $\chi^{(3)}/\alpha_0$. As for the absorption coefficient α_0, we take a model form combining the Lorentzian shape in the higher-energy side and the Urbach tail in the lower-energy side, namely

$$\alpha_0(\omega)=\begin{cases}\dfrac{1}{\pi}\dfrac{\gamma_{eg}}{(\omega-\omega_{eg})^2+\gamma_{eg}^2}, & \omega>\omega_{eg} \\ \dfrac{1}{\pi\gamma_{eg}}\exp(-|\omega-\omega_{eg}|/\gamma_{eg}), & \omega<\omega_{eg} \ .\end{cases} \tag{6.16}$$

The results are shown in Fig. 18. In the case of $\gamma_{bg}/\gamma_{eg}=0.1$, sharp structures are seen at the biexciton resonance. The figure of merit $|\chi^{(3)}|/\alpha_0$ at the two-photon resonance is about twice as large as that at the one-photon resonance, although the magnitude of $\chi^{(3)}$ itself at the two-photon resonance is smaller than that at the one-photon resonance. Even when the dephasing rate γ_{bg} is increased ($\gamma_{bg}/\gamma_{eg}=1.0$), the figure of merit at the two-photon resonance is still comparable to that at the one-photon resonance, as shown in Fig. 19, although the above sharp structures are smeared out. Furthermore, the response time of optical nonlinearity via the two-photon coherence of the biexciton state is determined mainly by the dephasing constant γ_{bg} and is expected to be very fast because the saturation mechanism of exciton population is not relevant. These features demonstrate most clearly the advantage of two-photon resonant excitation of the biexciton state in enhancing the optical nonlinearity.

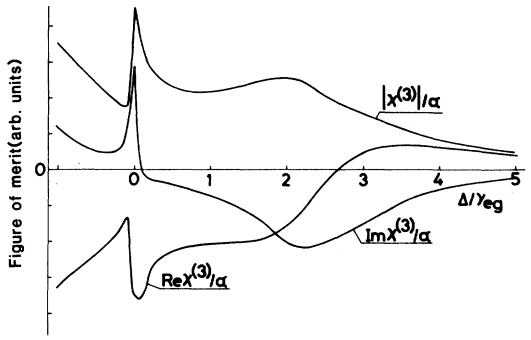

FIG. 18. Figure of merit of the third-order optical nonlinearity $\chi^{(3)}/\alpha$. The parameters are the same as in Fig. 16.

B. Two-photon absorption of the biexciton

As mentioned in the preceding section, the oscillator strength of transition from exciton to biexciton states is very large in semiconductor microcrystallites. As a consequence, the two-photon absorption coefficient of the biexciton can be also enhanced. Experimentally, one of the most direct evidences of the biexciton state is the observation of two-photon absorption. The two-photon absorption coefficient is related to $\chi^{(3)}(\omega;-\omega,-\omega,\omega)$, namely

$$\alpha(\omega)=\frac{4\pi\omega}{c(\epsilon_0)^{1/2}}\mathrm{Im}\chi^{(3)}|E(\omega)|^2 \ . \tag{6.17}$$

Around the two-photon resonance, $2\omega\cong\omega_{bg}$, $\chi^{(3)}$ can be approximated as given in (6.9),

$$\chi^{(3)}(2\omega\cong\omega_{bg})\cong\frac{i2|\mu_{eg}|^2|\mu_{be}|^2}{\hbar\gamma_{bg}B_{XX}^2}N \ , \tag{6.18}$$

where N is the number density of semiconductor microcrystallites. As seen from (6.17), the two-photon absorption coefficient is proportional to the incident power $I(\omega)$. Thus a more fundamental quantity which depends

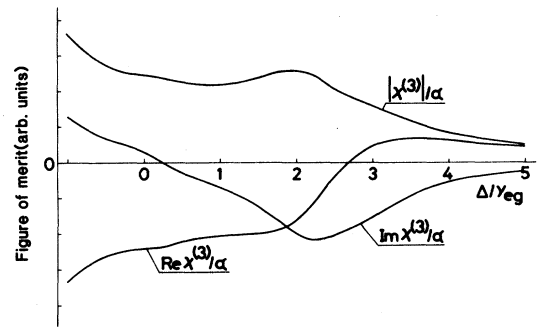

FIG. 19. Figure of merit of the third-order optical nonlinearity $\chi^{(3)}/\alpha$. The parameters are the same as in Fig. 16 except that $\gamma_{bg}/\gamma_{eg}=1.0$.

only on material parameters will be introduced by

$$K_2(\omega)=\frac{\alpha(\omega)}{I(\omega)}=\frac{32\pi^2\omega}{c^2\epsilon_0}\mathrm{Im}\chi^{(3)}\ , \tag{6.19}$$

where $I(\omega)$ is given in (F7). This is exactly equal to $\alpha_2(\omega)$ in (6.11). $K_2(\omega)$ is positive definite because $\mathrm{Im}\chi^{(3)}$ is positive, as given in (6.18). The values of K_2 will be given for typical materials in the next section.

VII. TYPICAL MATERIALS

Finally, we will discuss some typical materials which are promising for observing the biexciton state in microcrystallites. The first candidate is the $CdS_{1-x}Se_x$ mixed semiconductor microcrystallites embedded in a glass matrix, which seem to be realized in a semiconductor-doped filter glass. For CdS microcrystallites in a glass matrix, the relevant parameters are given as[31]

$$m_e/m_h\cong 0.24,\quad \epsilon_1/\epsilon_2\cong 3.8,\quad f_0\cong 8.14\ . \tag{7.1}$$

For a particle radius of $R/a_B=1$, i.e., $R\cong 30$ Å, the biexciton binding energy B_{XX} is estimated to be about 56 meV. This binding energy is about 14 times as large as that in bulk CdS (Refs. 32 and 33) and is sufficient to ensure the stability at room temperature. The oscillator strength of the exciton and biexciton states are calculated as

$$f_X/f_0\cong 5.2,\quad f_{XX}/f_0\cong 4.1\ . \tag{7.2}$$

Another example is a GaAs microcrystallite in vacuum with the relevant parameters[34]

$$m_e/m_h\cong 0.14,\quad \epsilon_1/\epsilon_2\cong 12.6,\quad f_0\cong 19.0\ . \tag{7.3}$$

Actually, this type of sample is realized in GaAs quantum disks patterned by electron-beam lithography,[35] in GaAs quantum boxes patterned by focused ion beam[36] and in GaInAsP/InP quantum-box structures fabricated by holographic lithography,[37] although the surrounding medium is not vacuum in these cases. For a particle radius of $R/a_B=0.2$, i.e., $R\cong 27$ Å, we obtain

$$B_{XX}\cong 46\ \text{meV},\quad f_X/f_0\cong 2.6,\quad f_{XX}/f_0\cong 2.3\ . \tag{7.4}$$

This binding energy is about 90 times as large as that in bulk GaAs (Ref. 29) and about twice as large as the thermal energy at room temperature ($k_BT\simeq 26$ meV).

The third candidate is a CuCl microcrystallite embedded in a NaCl matrix with the relevant parameters[31]

$$m_e/m_h\cong 0.22,\quad \epsilon_1/\epsilon_2\cong 2.3,\quad f_0\cong 5.90\ . \tag{7.5}$$

The small-angle x-ray-scattering data reveal that the shape of CuCl microcrystallites is flakelike rather than spherical.[38,39] These microcrystallites may more appropriately be called quantum disks than quantum dots. However, the effect of microcrystallite shape on the biexciton binding energy and on the optical properties may be small, as long as the microcrystallite size is larger than the exciton Bohr radius or the biexciton radius. This seems to be the case for actual samples of CuCl microcrystallite in NaCl. For a CuCl particle with radius of $R/a_B=3$, i.e., $R\cong 20$ Å, we estimate

$$B_{XX}\cong 114\ \text{meV},\quad f_X/f_0\cong 28.6,\quad f_{XX}/f_0\cong 22.4\ . \tag{7.6}$$

This binding energy is about 3 times as large as that in bulk CuCl (Refs. 40 and 41) and is much larger than the thermal energy at room temperature. This favors a CuCl microcrystallite as being one of the most promising samples for observing the biexciton state in microcrystallites. Most recently, Itoh[42] has observed successfully the biexciton state in this material and has obtained the biexciton binding energy of the same order as the predicted value.

Now the third-order nonlinear optical susceptibility $\chi^{(3)}$ will be calculated based on the formalism presented in the preceding section. Since the magnitude of $\chi^{(3)}$ depends sensitively on the relaxation constants, we must be careful in choosing the values of them. In the following, the longitudinal relaxation constant $\gamma_{\parallel}^{e}$ of the exciton state is identified with the inverse of radiative lifetime, namely

$$\gamma_{\parallel}^{e}=\frac{2ne^2\omega^2}{3m_0c^3}f_X\ . \tag{7.7}$$

The dephasing rate γ_{eg} can be determined from the homogeneous linewidth of the excitonic absorption spectrum. However, the other dephasing parameters γ_{be} and γ_{bg} are not well identified experimentally even in bulk materials. For CuCl crystals, the relaxation parameters γ_{eg}, γ_{be}, and γ_{bg} were determined through line-shape fitting of the resonant-Raman scattering spectra.[43] Thus, for the purpose of order estimation, we employ the following values, $\hbar\gamma_{eg}=\hbar\gamma_{be}=1$ meV, and $\hbar\gamma_{bg}=0.1$ meV, commonly for three materials. We found that the magnitude of $\chi^{(3)}$ is not very strongly dependent on these parameters around the above values. Employing a typical particle number density N of 10^{15} cm^{-3}, we estimated the magnitude of $\chi^{(3)}$ for both the one- and two-photon resonances and listed the results in Table I. $\chi^{(3)}$ values at the one-photon resonance are quite large and comparable to that of GaAs quantum-well structures.[44] On the other hand, $\chi^{(3)}$ values at the two-photon resonance are of the order of 10^{-9}–10^{-7} esu. As mentioned before, the magnitude of $\chi^{(3)}$ is proportional to the square of the oscillator strength and in turn the oscillator strength is determined by the smaller value of the microcrystallite volume and the coherence volume. Since, at the same time, the magnitude of $\chi^{(3)}$ is proportional to the particle number density, it may be possible to realize a $\chi^{(3)}$ value of the order of 0.1 or 1 esu by choosing an optimum particle size and by increasing the particle number density.

The two-photon absorption coefficients of these materials are estimated by employing the dephasing constant $\hbar\gamma_{bg}$ of 0.1 meV in (6.19) and are listed in Table I. These values will yield an easily measurable absorption coefficient for an incident power of 1 MW/cm^2. The estimated value of K_2 for CuCl microcrystallites is about an order of magnitude smaller than the observed values of K_2 for bulk samples of CuCl.[45,46] However, in consideration of the small volume fraction of microcrystallites about 0.1%, a dense packing of microcrystallites will possibly lead to a 2-order-of-magnitude enhancement of K_2 over the bulk value.

TABLE I. Material parameters and theoretical estimates of the biexciton binding energy B_{XX}, the third-order optical nonlinearity $\chi^{(3)}$ at the one- and two-photon resonances, and the two-photon absorption coefficient K_2 for typical semiconductor microcrystallites.

	GaAs in vacuum	CdS in glass	CuCl in NaCl
m_e/m_h	0.14	0.24	0.22
ϵ_1/ϵ_2	12.6	3.8	2.3
R (Å)	27	30	20
R/a_B	0.2	1.0	3.0
B_{XX} (meV)	46	56	114
B_{XX} (bulk, meV)	0.5	4.4	34
$\chi^{(3)}$ (esu) (one photon)	1.0×10^{-3}	6.8×10^{-5}	2.1×10^{-4}
$\chi^{(3)}$ (esu) (two photon)	1.3×10^{-7}	7.7×10^{-9}	1.2×10^{-8}
K_2 (cm/W)	4.2×10^{-5}	1.7×10^{-5}	7.2×10^{-5}

VIII. CONCLUSIONS

Biexciton states in semiconductor quantum dots are investigated variationally and dependences of their binding energy and oscillator strength on the quantum-dot radius (R), the electron-to-hole mass ratio (m_e/m_h), and the dielectric-constant ratio (ϵ_1/ϵ_2) are clarified for the first time. Most importantly, the significance of the dielectric confinement effect in enhancing the biexciton binding energy and the oscillator strength is demonstrated. It is found that in order to obtain a large biexciton binding energy it is favorable to choose an optimum value of R, a small value of m_e/m_h, and a large value of ϵ_1/ϵ_2. On the other hand, in order to obtain a large oscillator strength, it is advantageous to choose a large value of R, a small value of m_e/m_h, and an optimum value of ϵ_1/ϵ_2. For typical materials which are promising for observation of the biexciton state in microcrystallites, the values of the biexciton binding energy, the third-order nonlinear susceptibility $\chi^{(3)}$, and the two-photon absorption coefficient K_2 of the biexciton state are predicted theoretically.

A paper by Banyai *et al.*[47] has recently appeared which discusses the nonlinear optical properties of the biexciton state in semiconductor quantum dots. In their paper the biexciton binding energy is not given explicitly and its dependence on physical parameters is not examined systematically. We would, however, like to mention a few words on the results found by Banyai *et al.* in comparison with our results. They conclude that in the moderate confinement regime the biexciton energy is larger than twice the exciton energy, even when the dielectric effect is included; namely, the biexciton binding energy is negative. The moderate confinement regime is specified by

$$\frac{\sigma}{1+\sigma} < \frac{R}{a_B} < \frac{1}{1+\sigma} ,$$

where σ is the electron-to-hole mass ratio, and a_B is the exciton Bohr radius. For realistic values of σ, the above range is overlapping with the range discussed in the present paper. Thus their conclusion that the biexciton binding energy is negative in the moderate confinement regime is contradictory to our result. Their calculation in that regime is based on the adiabatic approximation, in which the holes are assumed to be moving in the average Coulomb potential due to the strongly confined electrons. Furthermore, they introduce a harmonic approximation for the effective hole-hole potential. These approximations lead to an oversimplification of the problem and are likely to discard the important part of correlation energy among electrons and holes, which may lower the biexciton energy. On the other hand, our variational approach treats all the energy terms on an equal footing without any approximations, at the cost of more involved algebra. Thus, the above discrepancy may arise from the difference in the theoretical approach. However, we believe that our results are more reliable than theirs because our variational approach has not introduced various simplifying approximations.

In our variational wave function, only the lowest subband levels are included as the envelope function associated with the electron-hole four-particle correlation function. This type of variational wave function is usually thought to be applicable only for the strong confinement regime. However, we found, surprisingly enough, that the variational wave function including only the lowest subband levels gives a very accurate estimate of the exciton energy, not only for the strong confinement regime, but also for the intermediate and even for the weak confinement regimes, in particular, for the particle radius up to several times the exciton Bohr radius. The difference in the energy eigenvalue from the result of a more elaborate calculation which includes many of the higher subbands is only a few percent, although in the eigenfunction the higher subband states begin to contribute substantially at the particle radius of a few times the exciton Bohr radius. Thus, for the biexciton state also, the present variational wave function is expected to give a very good estimate of the energy eigenvalue even for the intermediate (moderate) confinement regime.

Banyai *et al.* also discuss the effect of the dielectric constant difference between the semiconductor particle and the surrounding medium. They say that the absence of the dielectric effect causes the increasing difference between the biexciton energy E_2 and twice the exciton energy $2E_1$. In our understanding, the dielectric effect causes the enhancement of the Coulomb interaction and consequently increases the exciton and also the biexciton binding energies as long as the dielectric constant of the semiconductor is higher than that of the surrounding medium. Since in the case of Banyai *et al.* the biexciton binding energy is negative, we can assume that the absence of the dielectric effect raises the biexciton energy by an amount more than twice the increase in the exciton energy and hence causes the increasing E_2-2E_1.

ACKNOWLEDGMENTS

The author would like to thank Professor T. Itoh of Tohoku University for showing him experimental data prior to publication and for helpful discussions and Dr. T. Kimura for critical reading of the manuscript.

APPENDIX A: EXPRESSIONS OF G_l, F_l, H_l, P_l, AND $G_l^{\pm}$

G_l is defined by

$$G_l(x_a,x_b;\alpha)=\int_0^\infty dk\ k^2 g(k,\alpha) j_l(kx_a) j_l(kx_b)\ , \tag{A1}$$

with

$$g(k,\alpha)=\frac{\alpha}{\pi^2(k^2+\alpha^2)^2}\ , \tag{A2}$$

where j_l is the lth-order spherical Bessel function. Noticing the relation $j_l(x)=\frac{1}{2}[h_l^{(1)}(x)+h_l^{(2)}(x)]$ and making use of the analyticity of $h_l^{(1)}(h_l^{(2)})$ in the upper (lower) half-plane of x, we obtain

$$G_l(x_a,x_b;\alpha)=\frac{1}{4\pi}[h_l^{(1)}(i\alpha x_>) j_l(i\alpha x_<)+i\alpha x_> h_l^{(1)\prime}(i\alpha x_>) j_l(i\alpha x_<)+i\alpha x_< h_l^{(1)}(i\alpha x_>) j_l'(i\alpha x_<)]\ , \tag{A3}$$

where $x_>=\max(x_a,x_b)$ and $x_<=\min(x_a,x_b)$. These spherical Bessel and Hankel functions for pure imaginary arguments can be written in terms of modified Bessel functions. However, it is more convenient numerically to rewrite them by the following expressions:

$$j_l(ix)=(2ix)^l J_l^{R(0)}(x),\quad h_l^{(1)}(ix)=iH_l^{R(0)}(x)/(2ix)^{l+1}\ , \tag{A4}$$

$$j_l'(ix)=(2ix)^{l-1} J_l^{R(1)}(x),\quad h_l^{(1)\prime}(ix)=iH_l^{R(1)}(x)/(2ix)^{l+2}\ , \tag{A5}$$

$$j_l''(ix)=(2ix)^{l-2} J_l^{R(2)}(x),\quad h_l^{(1)\prime\prime}(ix)=iH_l^{R(2)}(x)/(2ix)^{l+3}\ , \tag{A6}$$

and so on. The explicit expressions of $J_l^{R(k)}(x), H_l^{R(k)}(x)$ $(k=0,1,2,\dots)$ are given in Appendix B. Then we have

$$G_l(x_a,x_b;\alpha)=\frac{1}{8\pi\alpha x_>}\left[\frac{x_<}{x_>}\right]^l\{H_l^{R(0)}(\alpha x_>) J_l^{R(0)}(\alpha x_<)+\tfrac{1}{2}[H_l^{R(1)}(\alpha x_>) J_l^{R(0)}(\alpha x_<) + H_l^{R(0)}(\alpha x_>) J_l^{R(1)}(\alpha x_<)]\}\ . \tag{A7}$$

Similarly, the function F_l, defined by

$$F_l(x_a,x_b;\alpha)=\int_0^\infty dk\ k^2 f(k,\alpha) j_l(kx_a) j_l(kx_b)\ , \tag{A8}$$

with

$$f(k,\alpha)=\frac{1}{2\pi^2(k^2+\alpha^2)}\ , \tag{A9}$$

is calculated as

$$-\frac{1}{8\pi}\frac{x_<^l}{x_>^{l+1}} H_l^{R(0)}(\alpha x_>) J_l^{R(0)}(\alpha x_<)\ . \tag{A10}$$

The function H_l defined by

$$H_l(x_a,x_b;\gamma,\delta)=\int_0^\infty dk\ k^2 h(k,\gamma,\delta) j_l(kx_a) j_l(kx_b)\ , \tag{A11}$$

with

$$h(k,\gamma,\delta)=\frac{\Gamma(2+\gamma)}{(2\pi)^2 ik}\left[\frac{1}{(\delta-ik)^{2+\gamma}}-\frac{1}{(\delta+ik)^{2+\gamma}}\right]\ , \tag{A12}$$

can be calculated in the same way as above for non-negative integers of γ. For $\gamma=0$, $H_l(x_a,x_b;0;\delta)$ reduces exactly to $G_l(x_a,x_b;\delta)$. For example, we find

$$H_l(x_a,x_b;1,\delta)=-\frac{1}{32\pi\delta^2}\frac{x_<^l}{x_>^{l+1}}\{4[H_l^{R(1)}(\delta x_>) J_l^{R(0)}(\delta x_<)+H_l^{R(0)}(\delta x_>) J_l^{R(1)}(\delta x_<)]+H_l^{R(2)}(\delta x_>) J_l^{R(0)}(\delta x_<) + 2H_l^{R(1)}(\delta x_>) J_l^{R(1)}(\delta x_<)+H_l^{R(0)}(\delta x_>) J_l^{R(2)}(\delta x_<)\}\ , \tag{A13}$$

$$H_l(x_a,x_b;2,\delta)=\frac{1}{64\pi\delta^3}\frac{x_<^l}{x_>^{l+1}}\{6[H_l^{R(2)}(\delta x_>) J_l^{R(0)}(\delta x_<)+2H_l^{R(1)}(\delta x_>) J_l^{R(1)}(\delta x_<)+H_l^{R(0)}(\delta x_>) J_l^{R(2)}(\delta x_<)] + H_l^{R(3)}(\delta x_>) J_l^{R(0)}(\delta x_<)+3H_l^{R(2)}(\delta x_>) J_l^{R(1)}(\delta x_<)+3H_l^{R(1)}(\delta x_>) J_l^{R(2)}(\delta x_<) + H_l^{R(0)}(\delta x_>) J_l^{R(3)}(\delta x_<)\}\ . \tag{A14}$$

More generally, for non-negative integer values of γ, setting $n=2+\gamma$, we find that

$$\int_0^\infty dk\, k^2 h(k,\gamma,\delta) j_l(kx_a) j_l(kx_b) = \frac{(-1)^n}{4\pi} \frac{d^{n-1}}{d\delta^{n-1}} [\delta h_l^{(1)}(i\delta x_>) j_l(i\delta x_<)] , \tag{A15}$$

and we can derive that

$$\frac{d^n}{d\delta^n}[\delta h_l^{(1)}(i\delta x_>) j_l(i\delta x_<)] = \frac{1}{(2\delta)^n} \frac{x_<^l}{x_>^{l+1}} \left\{ \tfrac{1}{2} \sum_{r=0}^{n} {}_nC_r H_l^{R(r)}(\delta x_>) J_l^{R(n-r)}(\delta x_<) + n \sum_{r=0}^{n-1} {}_{n-1}C_r H_l^{R(r)}(\delta x_>) J_l^{R(n-1-r)}(\delta x_<) \right\} . \tag{A16}$$

Now it is easy to derive a formula for P_l defined by

$$P_l(x_a,x_b;\gamma,\delta) = \int_0^\infty dk\, k^3 h(k,\gamma,\delta) j_l'(kx_a) j_l(kx_b) , \tag{A17}$$

with the same function h as given in (A12), if one notices that

$$P_l(x_a,x_b;\gamma,\delta) = \frac{d}{dx_a} \int_0^\infty dk\, k^2 h(k,\gamma,\delta) j_l(kx_a) j_l(kx_b) = \frac{(-1)^n}{4\pi} \frac{d}{dx_a} \frac{d^{n-1}}{d\delta^{n-1}} [\delta h_l^{(1)}(i\delta x_>) j_l(i\delta x_<)] , \tag{A18}$$

where γ is a non-negative integer and $n=2+\gamma$. After some manipulation we get a general formula

$$\frac{d}{dx_a}\frac{d^n}{d\delta^n}[\delta h_l^{(1)}(i\delta x_a) j_l(i\delta x_b)] = \frac{1}{(2\delta)^n} \frac{x_b^l}{x_a^{l+2}} \left\{ \tfrac{1}{2} \sum_{r=0}^{n} {}_nC_r [r H_l^{R(r)}(\delta x_a) + \tfrac{1}{2} H_l^{R(r+1)}(\delta x_a)] J_l^{R(n-r)}(\delta x_b) + n \sum_{r=0}^{n-1} {}_{n-1}C_r [r H_l^{R(r)}(\delta x_a) + \tfrac{1}{2} H_l^{R(r+1)}(\delta x_a)] J_l^{R(n-1-r)}(\delta x_b) \right\} \tag{A19}$$

for $x_a > x_b$, and

$$\frac{d}{dx_a}\frac{d^n}{d\delta^n}[\delta h_l^{(1)}(i\delta x_b) j_l(i\delta x_a)] = \frac{1}{(2\delta)^n} \frac{x_a^{l-1}}{x_b^{l+1}} \left\{ \tfrac{1}{2} \sum_{r=0}^{n} {}_nC_r [r J_l^{R(r)}(\delta x_a) + \tfrac{1}{2} J_l^{R(r+1)}(\delta x_a)] H_l^{R(n-r)}(\delta x_b) + n \sum_{r=0}^{n-1} {}_{n-1}C_r [r J_l^{R(r)}(\delta x_a) + \tfrac{1}{2} J_l^{R(r+1)}(\delta x_a)] H_l^{R(n-1-r)}(\delta x_b) \right\} \tag{A20}$$

for $x_a < x_b$. Using these formulas, $P_l(x_a,x_b;\gamma,\delta)$ can be calculated straightforwardly. For example, for $\gamma=2$, we have

$$\begin{aligned} P_l(x_a,x_b;2,\delta) &= \int_0^\infty dk\, k^3 h(k,2,\delta) j_l'(kx_a) j_l(kx_b) \\ &= \frac{1}{32\pi\delta^3} \frac{x_b^l}{x_a^{l+2}} \{ 6[H_l^{R(2)}(\delta x_a) J_l^{R(0)}(\delta x_b) + H_l^{R(1)}(\delta x_a) J_l^{R(1)}(\delta x_b)] \\ &\quad + 3[H_l^{R(3)}(\delta x_a) J_l^{R(0)}(\delta x_b) + 2H_l^{R(2)}(\delta x_a) J_l^{R(1)}(\delta x_b) + H_l^{R(1)}(\delta x_a) J_l^{R(2)}(\delta x_b)] \\ &\quad + \tfrac{1}{4}[H_l^{R(4)}(\delta x_a) J_l^{R(0)}(\delta x_b) + 3H_l^{R(3)}(\delta x_a) J_l^{R(1)}(\delta x_b) \\ &\quad + 3H_l^{R(2)}(\delta x_a) J_l^{R(2)}(\delta x_b) + H_l^{R(1)}(\delta x_a) J_l^{R(3)}(\delta x_b)] \} \end{aligned} \tag{A21}$$

for $x_a > x_b$, and

$$\begin{aligned} &\frac{1}{32\pi\delta^3} \frac{x_a^{l-1}}{x_b^{l+1}} \{ 6[J_l^{R(2)}(\delta x_a) H_l^{R(0)}(\delta x_b) + J_l^{R(1)}(\delta x_a) H_l^{R(1)}(\delta x_b)] \\ &\quad + 3[J_l^{R(3)}(\delta x_a) H_l^{R(0)}(\delta x_b) + 2J_l^{R(2)}(\delta x_a) H_l^{R(1)}(\delta x_b) + J_l^{R(1)}(\delta x_a) H_l^{R(2)}(\delta x_b)] \\ &\quad + \tfrac{1}{4}[J_l^{R(4)}(\delta x_a) H_l^{R(0)}(\delta x_b) + 3J_l^{R(3)}(\delta x_a) H_l^{R(1)}(\delta x_b) + 3J_l^{R(2)}(\delta x_a) H_l^{R(2)}(\delta x_b) \\ &\quad + J_l^{R(1)}(\delta x_a) H_l^{R(3)}(\delta x_b)] \} \end{aligned} \tag{A22}$$

for $x_a < x_b$.

In a similar way we can calculate $G_l^{\pm}(x_a,x_b;\alpha)$ in (3.50). Here we derive the expression for a more general integral defined by

$$G_{n,m}(x_a,x_b;\alpha) = \int_0^\infty dk \frac{k^3}{(k^2+\alpha^2)^2} j_n(kx_a) j_m(kx_b) , \tag{A23}$$

where integer numbers n and m are different by an odd number. We note that $G_{n,n\pm1}(x_a,x_b;\alpha)=G_n^{\pm}(x_a,x_b;\alpha)$. The above integral is calculated as

$$-\frac{\pi}{4}(2i\alpha)^{m-n-1}\frac{x_b^m}{x_a^{n+1}}\{2H_n^{R(0)}(\alpha x_a)J_m^{R(0)}(\alpha x_b)+\tfrac{1}{2}[H_n^{R(1)}(\alpha x_a)J_m^{R(0)}(\alpha x_b)+H_n^{R(0)}(\alpha x_a)J_m^{R(1)}(\alpha x_b)]\} \tag{A24}$$

for $x_a>x_b$, and

$$-\frac{\pi}{4}(2i\alpha)^{n-m-1}\frac{x_a^n}{x_b^{m+1}}\{2J_n^{R(0)}(\alpha x_a)H_m^{R(0)}(\alpha x_b)+\tfrac{1}{2}[J_n^{R(1)}(\alpha x_a)H_m^{R(0)}(\alpha x_b)+J_n^{R(0)}(\alpha x_a)H_m^{R(1)}(\alpha x_b)]\} \tag{A25}$$

for $x_a<x_b$.

APPENDIX B: SPHERICAL BESSEL AND HANKEL FUNCTIONS FOR PURE IMAGINARY ARGUMENTS

In this appendix, a numerical algorithm to calculate the spherical Bessel and Hankel functions for pure imaginary arguments is presented. From the power-series expansion of the spherical Bessel function[27]

$$j_n(z)=(2z)^n\sum_{m=0}^{\infty}\frac{(-1)^m(n+m)!}{m!(2n+2m+1)!}z^{2m}, \tag{B1}$$

we find

$$j_n(ix)=(2ix)^n\sum_{m=0}^{\infty}\frac{(n+m)!x^{2m}}{m!(2n+2m+1)!}, \tag{B2}$$

$$j_n'(ix)=2(2ix)^{n-1}\sum_{m=0}^{\infty}\frac{(n+m)!(2m+n)x^{2m}}{m!(2n+2m+1)!}, \tag{B3}$$

and

$$j_n''(ix)=4(2ix)^{n-2}\sum_{m=0}^{\infty}\frac{(n+m)!(2m+n)(2m+n-1)x^{2m}}{m!(2n+2m+1)!}. \tag{B4}$$

More generally, the pth derivative of the spherical Bessel function is given by

$$\begin{aligned}j_n^{(p)}(ix)&=(2ix)^{n-p}J_n^{R(p)}(x)\\&=(2ix)^{n-p}2^p\sum_{m=0}^{\infty}\frac{(n+m)!(2m+n)(2m+n-1)\cdots(2m+n-p+1)x^{2m}}{m!(2n+2m+1)!},\end{aligned} \tag{B5}$$

and $J_n^{R(p)}(x)$ is defined by this expression.

With respect to the spherical Hankel function, it is convenient to start from the power-series expansion[27]

$$h_n^{(1)}(z)=(-i)^{n+1}\frac{e^{iz}}{z}\sum_{r=0}^{n}\frac{(n+r)!}{r!(n-r)!}\left[\frac{i}{2z}\right]^r. \tag{B6}$$

Then we have

$$h_n^{(1)}(ix)=-\frac{2ie^{-x}}{(2ix)^{n+1}}\sum_{r=0}^{n}\frac{(2n-r)!}{r!(n-r)!}(2x)^r, \tag{B7}$$

$$h_n^{(1)'}(ix)=\frac{4ie^{-x}}{(2ix)^{n+2}}\sum_{r=0}^{n}\frac{(2n-r)!}{r!(n-r)!}(x+n-r+1)(2x)^r, \tag{B8}$$

and

$$h_n^{(1)''}(ix)=-\frac{8ie^{-x}}{(2ix)^{n+3}}\sum_{r=0}^{n}\frac{(2n-r)!}{r!(n-r)!}[x^2+2(n-r+1)x+(n-r+1)(n-r+2)](2x)^r. \tag{B9}$$

More generally, we can derive

$$\begin{aligned}h_n^{(1)(p)}(ix)&=\frac{iH_n^{R(p)}(x)}{(2ix)^{n+p+1}}\\&=\frac{i(-2)^{p+1}e^{-x}}{(2ix)^{n+p+1}}\sum_{r=0}^{n}\frac{(2n-r)!}{r!(n-r)!}[x^p+{}_pC_1(n-r+1)x^{p-1}+\cdots\\&\qquad+{}_pC_k(n-r+1)(n-r+2)\cdots(n-r+k)x^{p-k}+\cdots\\&\qquad+(n-r+1)(n-r+2)\cdots(n-r+p)](2x)^r,\end{aligned} \tag{B10}$$

and this expression defines $H_n^{R(p)}(x)$.

APPENDIX C: INTEGRAL OF PRODUCTS OF THREE AND FOUR SPHERICAL HARMONICS

The integral of product of three spherical harmonics can be written in terms of the Clebsch-Gordan coefficients as[28]

$$(l,m|l',m',l'',m'')\equiv\int d\Omega\, Y^*_{lm}(\Omega)Y_{l'm'}(\Omega)Y_{l''m''}(\Omega)$$
$$=\delta_{m,m'+m''}\left[\frac{(2l'+1)(2l''+1)}{4\pi(2l+1)}\right]^{1/2}\langle l,0|l',0,l'',0\rangle\langle l,m|l',m',l'',m''\rangle\ . \tag{C1}$$

This is equivalent to the formula

$$Y_{l_1m_1}(\Omega)Y_{l_2m_2}(\Omega)\equiv\sum_{l=|l_1-l_2|}^{l_1+l_2}\left[\frac{(2l_1+1)(2l_2+1)}{4\pi(2l+1)}\right]^{1/2}\langle l,0|l_1,0,l_2,0\rangle\langle l,m|l_1,m_1,l_2,m_2\rangle Y_{lm}(\Omega)\ , \tag{C2}$$

where $m=m_1+m_2$. Making use of this formula twice, we can calculate the integral of product of four spherical harmonics as

$$(l_1,m_1,l_2,m_2|l_3,m_3,l_4,m_4)\equiv\int d\Omega\, Y^*_{l_1m_1}(\Omega)Y^*_{l_2m_2}(\Omega)Y_{l_3m_3}(\Omega)Y_{l_4m_4}(\Omega)$$
$$=\delta_{m_1+m_2,m_3+m_4}\sum_l\frac{[(2l_1+1)(2l_2+1)(2l_3+1)(2l_4+1)]^{1/2}}{4\pi(2l+1)}$$
$$\times\langle l,0|l_1,0,l_2,0\rangle\langle l,m|l_1,m_1,l_2,m_2\rangle\langle l,0|l_3,0,l_4,0\rangle\langle l,m|l_3,m_3,l_4,m_4\rangle, \tag{C3}$$

where $m=m_1+m_2=m_3+m_4$ and the sum of l is implied over the common interval of $(|l_1-l_2|,l_1+l_2)$ and $(|l_3-l_4|,l_3+l_4)$.

APPENDIX D: EXPRESSIONS OF G_l, F_l, AND $G_l^{\pm}$ FOR NEGATIVE EXPONENT

The calculation in Appendix A is carried out assuming implicitly that the exponent α is positive. However, the exponent can take a negative value, as mentioned in the text. Thus we have to extend the formalism in Appendix A to the case where the exponent is negative. In this case the Fourier transform is not well defined because of divergence at the infinity. However, since the interparticle distance $r_{ij}=|r_i-r_j|$ is less than the diameter of a quantum dot, i.e., $2R$, we can restrict the Fourier integral from 0 to $2R$ and obtain a finite integral. Then the function $g(k,\alpha)$ is replaced by $g(k,\alpha;R)$ given by

$$g(k,\alpha;R)=(2\pi)^{-3}\int_0^{2R}dr\, r^2e^{-\alpha r}\int d\Omega\, e^{i\mathbf{k}\cdot\mathbf{r}}$$
$$=\frac{1}{\pi^2}\left[\frac{\alpha}{(k^2+\alpha^2)^2}-\frac{Re^{-2\alpha R}}{k^2+\alpha^2}\left[\frac{\alpha}{k}\sin 2kR+\cos 2kR\right]-\frac{e^{-2\alpha R}}{(k^2+\alpha^2)^2}\left[\alpha\cos 2kR+(\alpha^2-k^2)\frac{\sin 2kR}{2k}\right]\right], \tag{D1}$$

where the first term in the square brackets corresponds to $g(k,\alpha)$. Similarly $f(k,\alpha)$ is replaced by

$$f(k,\alpha;R)=(2\pi)^{-3}\int_0^{2R}dr\, r^2\frac{e^{-\alpha r}}{r}\int d\Omega e^{i\mathbf{k}\cdot\mathbf{r}}=\frac{1}{2\pi^2}\left[\frac{1}{k^2+\alpha^2}-\frac{e^{-2\alpha R}}{k^2+\alpha^2}\left[\frac{\alpha}{k}\sin 2kR+\cos 2kR\right]\right]. \tag{D2}$$

Then we have

$$\int_0^{\infty}dk\, k^2g(k,\alpha;R)j_l(kx_a)j_l(kx_b)=G_l(x_a,x_b;\alpha)+\Theta(-\alpha)\frac{(-4\alpha^2x_ax_b)^l}{2\pi}$$
$$\times\{J_l^{R(0)}(|\alpha|x_a)J_l^{R(0)}(|\alpha|x_b)+\tfrac{1}{2}[J_l^{R(1)}(|\alpha|x_a)J_l^{R(0)}(|\alpha|x_b)$$
$$+J_l^{R(0)}(|\alpha|x_a)J_l^{R(1)}(|\alpha|x_b)]\}\ , \tag{D3}$$

and

$$\int_0^{\infty}dk\, k^2f(k,\alpha;R)j_l(kx_a)j_l(kx_b)=F_l(x_a,x_b;\alpha)+\Theta(-\alpha)\frac{|\alpha|(-4\alpha^2x_ax_b)^l}{2\pi}J_l^{R(0)}(|\alpha|x_a)J_l^{R(0)}(|\alpha|x_b)\ , \tag{D4}$$

where Θ is the Heaviside step function and G_l and F_l are given in Appendix A. It is quite interesting to note that these integrals are independent of R, although the integrands are dependent on R. Another integral which is necessary in the variational calculation is given by

$$\int_0^\infty dk\, k^3 g(k,\alpha;R) j_n(kx_a) j_m(kx_b) = G_{n,m}(x_a,x_b;\alpha) + \Theta(-\alpha)\frac{i|\alpha|}{\pi}(2i|\alpha|x_a)^n(2i|\alpha|x_b)^m \times \{J_n^{R(0)}(|\alpha|x_a)J_m^{R(0)}(|\alpha|x_b) + \tfrac{1}{4}[J_n^{R(1)}(|\alpha|x_a)J_m^{R(0)}(|\alpha|x_b) + J_n^{R(0)}(|\alpha|x_a)J_m^{R(1)}(|\alpha|x_b)]\}\ , \tag{D5}$$

where $G_{n,m}(x_a,x_b;\alpha)$ is given in Appendix A.

APPENDIX E: DERIVATION OF THE THIRD ORDER NONLINEAR SUSCEPTIBILITY $\chi^{(3)}$

The third-order nonlinear optical susceptibility $\chi^{(3)}$ is calculated employing a three-level model for the exciton-biexciton transitions. Hereafter, the ground state will be denoted by g, the excitonic state by e, and the biexciton state by b, respectively. The equation of motion for the density matrix is generally written as[48]

$$\dot{\rho} = -\frac{i}{\hbar}[H,\rho] + \Gamma\rho\ . \tag{E1}$$

The equations of motion for matrix elements are written explicitly as

$$\dot{\rho}_{eg} = (-i\omega_{eg} - \gamma_{eg})\rho_{eg} + \frac{iE(t)}{\hbar}[\mu_{eg}(\rho_{gg} - \rho_{ee}) + \mu_{eb}\rho_{bg}]\ , \tag{E2}$$

$$\dot{\rho}_{gg} = \gamma_{\parallel}^{e}\rho_{ee} + \frac{iE(t)}{\hbar}(\mu_{ge}\rho_{eg} - \mu_{eg}\rho_{ge})\ , \tag{E3}$$

$$\dot{\rho}_{ee} = -\gamma_{\parallel}^{e}\rho_{ee} + \gamma_{\parallel}^{b}\rho_{bb} + \frac{iE(t)}{\hbar}(\mu_{eg}\rho_{ge} - \mu_{ge}\rho_{eg} + \mu_{eb}\rho_{be} - \mu_{be}\rho_{eb})\ , \tag{E4}$$

$$\dot{\rho}_{bb} = -\gamma_{\parallel}^{b}\rho_{bb} + \frac{iE(t)}{\hbar}(\mu_{be}\rho_{eb} - \mu_{eb}\rho_{be})\ , \tag{E5}$$

$$\dot{\rho}_{be} = (-i\omega_{be} - \gamma_{be})\rho_{be} + \frac{iE(t)}{\hbar}[\mu_{be}(\rho_{ee} - \rho_{bb}) - \mu_{ge}\rho_{bg}]\ , \tag{E6}$$

$$\dot{\rho}_{bg} = (-i\omega_{bg} - \gamma_{bg})\rho_{bg} + \frac{iE(t)}{\hbar}(\mu_{be}\rho_{eg} - \mu_{eg}\rho_{be})\ , \tag{E7}$$

where ω_{ij} and μ_{ij} denote the frequency difference and transition dipole moment between i and j levels, respectively, and γ_{ij} is the dephasing rate of the transition dipole moment μ_{ij}. The trace of the density matrix is conserved, namely

$$\rho_{gg} + \rho_{ee} + \rho_{bb} = 1\ . \tag{E8}$$

For an electric field E given by

$$E(t) = \tfrac{1}{2}[E(\omega_1)e^{-i\omega_1 t} + E(\omega_2)e^{-i\omega_2 t} + \text{c.c.}]\ , \tag{E9}$$

we expand each matrix element in powers of E as

$$\rho_{ij} = \rho_{ij}^{(0)} + \rho_{ij}^{(1)} + \rho_{ij}^{(2)} + \cdots\ , \tag{E10}$$

with the initial condition that $\rho_{gg}^{(0)}(0) = 1$ and other matrix elements are zero. By the successive iteration of the perturbation expansion with respect to E,[49] we obtain

$$\rho_{eg}^{(1)}(t) = \frac{i\mu_{eg}}{\hbar}\int_0^t d\tau \exp[(-i\omega_{eg} - \gamma_{eg})(t-\tau)]E(\tau)\ , \tag{E11}$$

$$\rho_{ee}^{(2)}(t) = \frac{|\mu_{eg}|^2}{\hbar^2}\int_0^t dt_1 \int_0^{t_1} dt_2 \exp[-\gamma_{\parallel}^{e}(t-t_1) + (-i\omega_{eg} - \gamma_{eg})(t_1 - t_2)]E(t_1)E(t_2) + \frac{|\mu_{eg}|^2}{\hbar^2}\int_0^t dt_1 \int_0^{t_1} dt_2 \exp[-\gamma_{\parallel}^{e}(t-t_1) + (i\omega_{eg} - \gamma_{eg})(t_1 - t_2)]E(t_1)E(t_2)\ , \tag{E12}$$

$$\rho_{gg}^{(2)} = -\rho_{ee}^{(2)}\ , \tag{E13}$$

$$\rho_{bg}^{(2)}(t) = -\frac{\mu_{be}\mu_{eg}}{\hbar^2}\int_0^t dt_1 \int_0^{t_1} dt_2 \exp[(-i\omega_{bg} - \gamma_{bg})(t-t_1) + (-i\omega_{eg} - \gamma_{eg})(t_1 - t_2)]E(t_1)E(t_2)\ , \tag{E14}$$

$$\rho_{eg}^{(3)}(t)=-\frac{2i|\mu_{eg}|^2\mu_{eg}}{\hbar^3}\int_0^t dt_1\int_0^{t_1}dt_2\int_0^{t_2}dt_3\exp[(-i\omega_{eg}-\gamma_{eg})(t-t_1)-\gamma_{\parallel}^{e}(t_1-t_2)$$
$$+(-i\omega_{eg}-\gamma_{eg})(t_2-t_3)]E(t_1)E(t_2)E(t_3)$$
$$-\frac{2i|\mu_{eg}|^2\mu_{eg}}{\hbar^3}\int_0^t dt_1\int_0^{t_1}dt_2\int_0^{t_2}dt_3\exp[(-i\omega_{eg}-\gamma_{eg})(t-t_1)-\gamma_{\parallel}^{e}(t_1-t_2)$$
$$+(i\omega_{eg}-\gamma_{eg})(t_2-t_3)]E(t_1)E(t_2)E(t_3)$$
$$-\frac{i|\mu_{be}|^2\mu_{eg}}{\hbar^3}\int_0^t dt_1\int_0^{t_1}dt_2\int_0^{t_2}dt_3\exp[(-i\omega_{eg}-\gamma_{eg})(t-t_1)+(-i\omega_{bg}-\gamma_{bg})(t_1-t_2)$$
$$+(-i\omega_{eg}-\gamma_{eg})(t_2-t_3)]E(t_1)E(t_2)E(t_3)\ , \tag{E15}$$

$$\rho_{be}^{(3)}(t)=\frac{i|\mu_{eg}|^2\mu_{be}}{\hbar^3}\int_0^t dt_1\int_0^{t_1}dt_2\int_0^{t_2}dt_3\exp[(-i\omega_{be}-\gamma_{be})(t-t_1)-\gamma_{\parallel}^{e}(t_1-t_2)$$
$$+(-i\omega_{eg}-\gamma_{eg})(t_2-t_3)]E(t_1)E(t_2)E(t_3)$$
$$+\frac{i|\mu_{eg}|^2\mu_{be}}{\hbar^3}\int_0^t dt_1\int_0^{t_1}dt_2\int_0^{t_2}dt_3\exp[(-i\omega_{be}-\gamma_{be})(t-t_1)-\gamma_{\parallel}^{e}(t_1-t_2)$$
$$+(i\omega_{eg}-\gamma_{eg})(t_2-t_3)]E(t_1)E(t_2)E(t_3)$$
$$+\frac{i|\mu_{eg}|^2\mu_{be}}{\hbar^3}\int_0^t dt_1\int_0^{t_1}dt_2\int_0^{t_2}dt_3\exp[(-i\omega_{be}-\gamma_{be})(t-t_1)+(-i\omega_{bg}-\gamma_{bg})(t_1-t_2)$$
$$+(-i\omega_{eg}-\gamma_{eg})(t_2-t_3)]E(t_1)E(t_2)E(t_3)\ . \tag{E16}$$

The third-order nonlinear polarization is given by

$$P^{(3)}=\mathrm{Tr}\mu\rho^{(3)}=\mu_{ge}\rho_{eg}^{(3)}+\mu_{eb}\rho_{be}^{(3)}+\mathrm{c.c.}\ . \tag{E17}$$

Extracting the polarization component with the time dependence of $e^{-i(2\omega_1-\omega_2)t}$, we define the third-order nonlinear susceptibility by

$$P^{(3)}(2\omega_1-\omega_2)=\tfrac{1}{2}[\chi^{(3)}(2\omega_1-\omega_2;-\omega_1,-\omega_1,\omega_2)E(\omega_1)E(\omega_1)E^*(\omega_2)e^{-i(2\omega_1-\omega_2)t}+\mathrm{c.c.}]\ . \tag{E18}$$

Then we have

$$\chi^{(3)}(2\omega_1-\omega_2;-\omega_1,-\omega_1,\omega_2)=-\frac{i|\mu_{eg}|^4}{2\hbar^3}\frac{1}{i(\omega_{eg}-2\omega_1+\omega_2)+\gamma_{eg}}\frac{1}{i(\omega_2-\omega_1)+\gamma_{\parallel}^{e}}$$
$$\times\left[\frac{1}{i(\omega_{eg}-\omega_1)+\gamma_{eg}}+\frac{1}{i(\omega_2-\omega_{eg})+\gamma_{eg}}\right]$$
$$-\frac{i|\mu_{eg}|^2|\mu_{be}|^2}{4\hbar^3}\frac{1}{i(\omega_{eg}-2\omega_1+\omega_2)+\gamma_{eg}}\frac{1}{i(\omega_{bg}-2\omega_1)+\gamma_{bg}}\frac{1}{i(\omega_{eg}-\omega_1)+\gamma_{eg}}$$
$$+\frac{i|\mu_{eg}|^2|\mu_{be}|^2}{4\hbar^3}\frac{1}{i(\omega_{be}-2\omega_1+\omega_2)+\gamma_{be}}\frac{1}{i(\omega_2-\omega_1)+\gamma_{\parallel}^{e}}$$
$$\times\left[\frac{1}{i(\omega_{eg}-\omega_1)+\gamma_{eg}}+\frac{1}{i(\omega_2-\omega_{eg})+\gamma_{eg}}\right]$$
$$+\frac{i|\mu_{eg}|^2|\mu_{be}|^2}{4\hbar^3}\frac{1}{i(\omega_{be}-2\omega_1+\omega_2)+\gamma_{be}}\frac{1}{i(\omega_{bg}-2\omega_1)+\gamma_{bg}}\frac{1}{i(\omega_{eg}-\omega_1)+\gamma_{eg}}\ . \tag{E19}$$

APPENDIX F: RELATIONS AMONG $\mathrm{Re}\chi^{(3)}$, $\mathrm{Im}\chi^{(3)}$, n_2, α_2, η_{eh}, AND σ_{eh}

The relations between the real and imaginary parts of $\chi^{(3)}$ and the nonlinear changes of refractive index η_{eh} and of absorption coefficient σ_{eh} per one electron-hole pair in a unit volume are derived. For a monochromatic electric field given by

$$E(t)=\tfrac{1}{2}[E(\omega)e^{-i\omega t}+\mathrm{c.c.}]\ , \tag{F1}$$

the third-order nonlinear polarization is written as

$$P^{(3)}(t)=\tfrac{1}{2}[P^{(3)}(\omega)e^{-i\omega t}+\text{c.c.}] , \tag{F2}$$

and the third-order nonlinear susceptibility $\chi^{(3)}(\omega)$ is defined by

$$P^{(3)}(\omega)=\chi^{(3)}(\omega)E(\omega)E(\omega)E^*(\omega) . \tag{F3}$$

The dielectric constant is given by

$$\begin{aligned}\epsilon&=1+4\pi\chi^{(1)}(\omega)+4\pi\chi^{(3)}(\omega)|E(\omega)|^2\\&=\epsilon_0+4\pi\chi^{(3)}(\omega)|E(\omega)|^2 ,\end{aligned} \tag{F4}$$

where ϵ_0 is the linear susceptibility. Then the refractive index n is defined by the real part of the square root of ϵ as

$$n+i\kappa=\sqrt{\epsilon}\cong n_0+\frac{2\pi\chi^{(3)}(\omega)}{n_0}|E(\omega)|^2 , \tag{F5}$$

with $n_0=(\epsilon_0)^{1/2}$. When ϵ_0 is assumed to be dominantly real, we have

$$n=n_0+\frac{2\pi\,\mathrm{Re}\chi^{(3)}(\omega)}{n_0}|E(\omega)|^2=n_0+n_2 I , \tag{F6}$$

where I is the incident power per unit area given by

$$I=\frac{c}{4\pi}\overline{E\times H}=\frac{cn_0}{8\pi}|E(\omega)|^2 . \tag{F7}$$

Thus the coefficient n_2 of nonlinear change of the refractive index is given by[50]

$$n_2=\frac{16\pi^2}{c\epsilon_0}\mathrm{Re}\chi^{(3)}(\omega) . \tag{F8}$$

To obtain η_{eh}, defined by

$$n=n_0+\eta_{eh}N , \tag{F9}$$

with the electron-hole pair density N per unit volume, we must relate N to I. The rate equation for N is given by

$$\dot{N}=\frac{\alpha}{\hbar\omega}I-\frac{N}{\tau} , \tag{F10}$$

where α is the absorption coefficient and τ is the population lifetime. This equation has a stationary solution

$$N=\frac{\alpha\tau}{\hbar\omega}I . \tag{F11}$$

Thus we find

$$\eta_{eh}=\frac{\hbar\omega}{\alpha\tau}n_2 . \tag{F12}$$

The absorption coefficient α is given by

$$\alpha(\omega)=\frac{4\pi\omega}{n_0 c}\mathrm{Im}\chi(\omega) , \tag{F13}$$

with

$$\chi(\omega)=\chi^{(1)}(\omega)+\chi^{(3)}(\omega)|E(\omega)|^2 . \tag{F14}$$

Then we have

$$\begin{aligned}\alpha&=\frac{4\pi\omega}{n_0 c}[\mathrm{Im}\chi^{(1)}(\omega)+\mathrm{Im}\chi^{(3)}(\omega)|E(\omega)|^2]\\&=\alpha_0+\alpha_2 I .\end{aligned} \tag{F15}$$

The coefficient α_2 of nonlinear change of the absorption coefficient is calculated as

$$\alpha_2=\frac{32\pi^2\omega}{c^2\epsilon_0}\mathrm{Im}\chi^{(3)}(\omega) . \tag{F16}$$

The absorption change σ_{eh} per one electron-hole pair in a unit volume is defined by

$$\alpha=\alpha_0+\sigma_{eh}N , \tag{F17}$$

and is given by

$$\sigma_{eh}=\frac{\hbar\omega}{\alpha\tau}\alpha_2 . \tag{F18}$$

Thus it is seen that the efficiencies of optical nonlinearity η_{eh} and σ_{eh} are proportional to the real and imaginary parts of $\chi^{(3)}/\alpha\tau$, respectively.

[1] Al. L. Efros and A. L. Efros, Fiz. Tekh. Poluprovodn. **16**, 1209 (1982) [Sov. Phys.—Semicond. **16**, 772 (1982)].
[2] A. I. Ekimov and A. A. Onushchenko, Fiz. Tekh. Poluprovodn. **16**, 1215 (1982) [Sov. Phys.—Semicond. **16**, 775 (1982)].
[3] A. I. Ekimov, Al. L. Efros, and A. A. Onushchenko, Solid State Commun. **56**, 921 (1985).
[4] L. E. Brus, J. Chem. Phys. **80**, 4403 (1984).
[5] L. E. Brus, IEEE J. Quantum Electron. **QE-22**, 1909 (1986).
[6] Y. Kayanuma, Solid State Commun. **59**, 405 (1986).
[7] S. V. Nair, S. Sinha, and K. C. Rustagi, Phys. Rev. B **35**, 4098 (1987).
[8] S. Schmitt-Rink, D. A. B. Miller, and D. S. Chemla, Phys. Rev. B **35**, 8113 (1987).
[9] T. Takagahara, Phys. Rev. B **36**, 9293 (1987).
[10] T. Takagahara, Surf. Sci. **196**, 590 (1987).
[11] E. Hanamura, Phys. Rev. B **37**, 1273 (1988).
[12] G. W. Bryant, Phys. Rev. B **37**, 8763 (1988).
[13] R. K. Jain and R. C. Lind, J. Opt. Soc. Am. **73**, 647 (1983).
[14] P. Roussignol, D. Ricard, and C. Flytzanis, Appl. Phys. A **44**, 285 (1987).
[15] J. Yumoto, S. Fukushima, and K. Kubodera, Opt. Lett. **12**, 832 (1987).
[16] M. Mitsunaga, H. Shinojima, and K. Kubodera, J. Opt. Soc. Am. B **5**, 1448 (1988).
[17] D. A. Kleinman, Phys. Rev. B **28**, 871 (1983).
[18] Q. Fu, D. Lee, A. Mysyrowicz, A. V. Nurmikko, R. L. Gunshor, and L. A. Kolodziejski, Phys. Rev. B **37**, 8791 (1988).
[19] L. Banyai, I. Galbraith, C. Ell, and H. Haug, Phys. Rev. B **36**, 6099 (1987).
[20] L. V. Keldysh, Pis'ma Zh. Eksp. Teor. Fiz. **29**, 716 (1979) [JETP Lett. **29**, 658 (1979)].
[21] E. Hanamura, N. Nagaosa, M. Kumagai, and T. Takagahara, Mater. Sci. Eng. B **1**, 255 (1988).
[22] T. Takagahara, in Technical Digest of the XVIth International Conference on Quantum Electronics (Tokyo, 1988), p. 620

(unpublished).
[23]L. Banyai, M. Lindberg, and S. W. Koch, Opt. Lett. **13**, 212 (1988).
[24]E. Hanamura, Solid State Commun. **12**, 951 (1973).
[25]Z. W. Fu and J. D. Dow, Bull. Am. Phys. Soc. **31**, 557 (1986).
[26]O. Akimoto and E. Hanamura, J. Phys. Soc. Jpn. **33**, 1537 (1972).
[27]M. Abramowitz and I. A. Stegun, *Handbook of Mathematical Functions,* 10th ed. (Dover, New York, 1972).
[28]E. U. Condon and G. H. Shortley, *The Theory of Atomic Spectra* (Cambridge University Press, Cambridge, England, 1970).
[29]G. W. 't Hooft, W. A. J. A. van der Poel, L. W. Molenkamp, and C. T. Foxon, Phys. Rev. B **35**, 8281 (1987).
[30]J. Feldmann, G. Peter, E. O. Göbel, P. Dawson, K. Moore, C. Foxon, and R. J. Elliott, Phys. Rev. Lett. **59**, 2337 (1987).
[31]*Physics of II-VI and I-VII Compounds, Semimagnetic Semiconductors,* Vol. 17b of *Landolt-Börnstein,* edited by O. Madelung, M. Schulz, and H. Weiss (Springer, Berlin, 1982).
[32]Y. Nozue, T. Itoh, and M. Ueta, J. Phys. Soc. Jpn. **44**, 1305 (1978).
[33]J. Puls, I. Rückmann, and J. Voigt, Phys. Status Solidi B **96**, 641 (1979).
[34]*Physics of Group IV Elements and III-V Compounds,* Vol. 17a of *Landolt-Börnstein,* edited by O. Madelung, M. Schulz, and H. Weiss (Springer, Berlin, 1982).
[35]K. Kash, A. Scherer, J. M. Worlock, H. G. Craighead, and M. C. Tamargo, Appl. Phys. Lett. **49**, 1043 (1986).
[36]J. Cibert, P. M. Petroff, G. J. Dolan, S. J. Pearton, A. C. Gossard, and J. H. English, Appl. Phys. Lett. **49**, 1275 (1986).
[37]Y. Miyamoto, M. Cao, Y. Shingai, K. Furuya, Y. Suematsu, K. G. Ravikumar, and S. Arai, Jpn. J. Appl. Phys. **26**, L225 (1987).
[38]T. Itoh, Y. Iwabuchi, and M. Kataoka, Phys. Status Solidi B **145**, 567 (1988).
[39]T. Itoh, Y. Iwabuchi, and T. Kirihara, Phys. Status Solidi B **146**, 531 (1988).
[40]G. M. Gale and A. Mysyrowicz, Phys. Rev. Lett. **32**, 727 (1974).
[41]N. Nagasawa, N. Nakata, Y. Doi, and M. Ueta, J. Phys. Soc. Jpn. **39**, 987 (1975).
[42]T. Itoh, in *Nonlinear Optics of Organics and Semiconductors,* edited by T. Kobayashi (Springer-Verlag, Berlin, in press).
[43]E. Hanamura and T. Takagahara, J. Phys. Soc. Jpn. **47**, 410 (1979).
[44]D. S. Chemla, D. A. B. Miller, P. W. Smith, A. C. Gossard, and W. Wiegmann, IEEE J. Quantum Electron. **QE-20**, 265 (1984).
[45]N. Nagasawa, T. Mita, and M. Ueta, J. Phys. Soc. Jpn. **41**, 929 (1976).
[46]Vu Duy Phach, A. Bivas, B. Hönerlage, and J. B. Grun, Phys. Status Solidi B **84**, 731 (1977).
[47]L. Banyai, Y. Z. Hu, M. Lindberg, and S. W. Koch, Phys. Rev. B **38**, 8142 (1988).
[48]N. Bloembergen, *Nonlinear Optics* (Benjamin, New York, 1965).
[49]T. Yajima and H. Souma, Phys. Rev. A **17**, 309 (1978).
[50]A similar derivation is given in H. B. Gibbs, *Optical Bistability: Controlling Light with Light* (Academic, New York, 1985).